# High-Efficiency Low-Dross Combustion System For Aluminum Remelting Reverberatory Furnaces

## Project Final Report

By
V. Soupos
S. Zelepouga
D. Rue

July 2005

Work Performed Under Contract No. DE-FC07-00ID13903

For U. S. Department Of Energy
Idaho Operations Office
850 Energy Drive, MS 1221
Idaho Falls, Idaho 83401-1563

By
Gas Technology Institute
1700 S. Mount Prospect Rd.
Des Plaines, Illinois 60018

## EXECUTIVE SUMMARY

This report presents the work performed by the Gas Technology Institute and subcontractors Eclipse Combustion, the University of Illinois at Chicago and Wabash Alloys, during the period from July 1, 2001 – June 30, 2002 under contract (No.: DE-FC07-00ID13903) with the U. S. Department of Energy.

GTI, and its commercial partners, have developed a high-efficiency low-dross combustion system that offers environmental and energy efficiency benefits at lower capital costs for the secondary aluminum industry users of reverberatory furnaces. The high-efficiency low-dross combustion system, also called Self-Optimizing Combustion System (SOCS), includes the flex-flame burner firing an air or oxygen-enriched natural gas flame, a non-contact optical flame sensor, and a combustion control system. The flex-flame burner, developed and tested by GTI, provides an innovative firing process in which the flame shape and velocity can be controlled. The burner produces a flame that keeps oxygen away from the bath surface by including an $O_2$-enriched fuel-rich zone on the bottom and an air-fired fuel-lean zone on the top. Flame shape and velocity can be changed at constant firing rate or held constant over a range of firing conditions. A non-intrusive optical sensor is used to monitor the flame at all times. Information from the optical sensor(s) and thermocouples can be used to control the flow of natural gas, air, and oxygen to the burner as needed to maintain desired flame characteristics. This type of control is particularly important to keep oxygen away from the melt surface and thus reduce dross formation.

This retrofit technology decreases fuel usage, increases furnace production rate, lowers gaseous emissions, and reduces dross formation. The highest priority research need listed under Recycled Materials is to turn aluminum process waste into usable materials which this technology accomplishes directly by decreasing dross formation and therefore increasing aluminum yield from a gas-fired reverberatory furnace. Emissions of $NO_x$ will be reduced to approximately 0.3 lb/ton of aluminum, in compliance with air emission regulations.

The objective of this project is to develop the high-efficiency low-dross combustion system and to demonstrate this advanced combustion system on an industrial reverberatory furnace. At the completion of this project, with the aid of the Industrial Adoption Plan to be prepared and updated throughout the project, the technology will be ready for commercial application.

# FINAL REPORT

**Project Title**

High-Efficiency Low-Dross Combustion System for Aluminum Remelt Reverberatory Furnaces

**Covering Period**

June 15, 2000 through June 30, 2005

**Date of Report**

July 31, 2005

**Recipient**

Gas Technology Institute
1700 S. Mt. Prospect Rd.
Des Plaines, IL 60018

**Award Number**

DE-FC07-00ID13903

**Subcontractors**

University of Illinois at Chicago
Eclipse, Inc.

**Other Partners**

Southern California Gas Co. – project sponsor
GTI Sustaining Membership Program (SMP) – project sponsor
Wabash Alloys – industrial host site partner

**Contacts**

David M. Rue
Manager, Industrial Combustion Processes
Gas Technology Institute
847-768-0508
david.rue@gastechnology.org

Serguei Zelepouga
Principle Combustion Engineer
Gas Technology Institute
847-768-0580
Serguei.Zelepouga@gastechnology.org

**Project Team**

Sara Dillich
Aluminum Team Leader
U.S. Dept. of Energy
OIT, EE-20
1000 Independence Ave.,
Washington, DC 20585-0121
202-586-7925
sara.dillich@ee.doe.gov

John Yankeelov
U.S. Dept. of Energy
Idaho Operations Office
50 Energy Drive
Idaho Falls, ID 83401-1563
208-526-7049
yankeeja@id.doe.gov

Doreen K. Leonard
Reports Monitor
U.S. DOE, Idaho Operations Office
Office of Chief Financial Officer
Procurement Services Division
850 Energy Dr. / Mail Stop 1221
Idaho Falls, ID 83401-1563
leonarddk@id.doe.gov

TABLE OF CONTENTS

## PROJECT OBJECTIVE

The objective of this project is to develop and demonstrate the high-efficiency low-dross combustion system for reverberatory furnaces used for aluminum remelting.

Reverberatory furnaces typically have a low efficiency because the liquid aluminum reflects a large fraction of the available heat. The furnace refractory is heated, and radiation from the hot refractory heats the melt in the bath. Although a number of exhaust gas heat recovery techniques have been developed and employed, furnace efficiencies remain low, often at values around 25 percent. The objective of this project is to use an $O_2$-enriched combustion process with burners capable of flame shaped adjustment to provide significantly greater energy efficiency than present reverberatory furnaces combustion systems.

Economic and environmental analyses have found that the greatest cost savings from an improved combustion system are realized from the reduction in dross. Dross is largely aluminum oxide formed by reaction of oxygen with the molten aluminum. The high-efficiency low-dross combustion system decreases dross by an estimated 60 percent by blanketing the surface of the melt with an oxygen-free zone produced by a fuel-rich flame. This combustion system creates a flame that is oxygen-free and fuel rich on the bottom close to the bath surface and fuel-lean for CO and VOC burn-out on top. Dross is also reduced by controlling the temperature of the bath surface. Hot spots are the second major component in dross formation. This advanced combustion system eliminates the two leading causes of dross formation, oxygen contact with the molten aluminum and local hot spots on the surface of the bath.

Energy cost is less than 20 percent of the cost of secondary aluminum melting. Therefore, saving 40% of the natural gas required for heating and purchasing needed oxygen provides only a small economic benefit to the reverberatory furnace operator. Decreasing the dross, which also increases the aluminum yield per pound, decreases dross handling and processing, and decreases the amount of salt cake formed and subsequently sent for disposal. A key objective of this project is to develop a combustion system that improves process energy efficiency and economics by greatly reducing the amount of dross formed.

This project is divided into three 12-month long Phases, each consisting of five specific Tasks. The work involved in each Phase and Task is detailed in the table below.

**Table 1. Milestone Table**

| Phase | Task | Title | % complete |
|---|---|---|---|
| 1 | 1 | Laboratory Flame Testing | 100 |
| | 2 | Laboratory Burner Design and Fabrication | 100 |
| | 3 | Furnace and Sensor Preparation | 100 |
| | 4 | Laboratory Testing and Analysis | 100 |
| | 5 | Industrial Adoption Plan | 40 |
| 2 | 6 | Pilot Burner Design and Fabrication | 100 |
| | 7 | Combustion System Integration | 100 |
| | 8 | Testing and Analysis | 100 |
| | 9 | Host Site Selection | 100 |
| | 10 | Industrial Adoption Plan | 40 |
| 3 | 11 | Furnace Baseline Measurements | 100 |
| | 12 | Demonstration System Design and Fabrication | 100 |
| | 13 | Combustion System Installation | 100 |
| | 14 | Testing and Analysis | 100 |
| | 15 | Industrial Adoption Plan | 0 |

The Phases are individually focused on laboratory testing of the SOCS system - tasks 1 through 4, pilot-scale testing of the components and the integrated SOCS system – tasks 5 through 9 (Phase I), and field testing to demonstrate industrial benefits of the technology – tasks 10 though 15 (Phase II). All work in Phase I and II is complete.

**WORK COMPLETED IN PHASE I, TASKS 1-4**

A laboratory-scale version of the SOCS was designed, fabricated, and installed at the GTI Applied Combustion Research Laboratory. This prototype can be fired at rates of 0.02 to 0.4 MM Btu/h. The SOCS was designed to allow adjustment of flame shape, flame length, and mixing patterns. This prototype was tested along with the optical flame sensor, which was also developed at GTI and is coupled with the SOCS. Besides the SOCS and the sensor, the experimental apparatus included controls from MKS Inc., gas flow meters, and a PC-based data acquisition system. The experimental apparatus used to generate the hybrid flames is depicted in Figure 1. Spectroscopic measurements of lean/rich flame patterns were supplemented with conventional flue gas analysis. A Horiba Combustion analyzer was used to measure flue gas compositions at two locations in the flame, as shown in Figure 2.

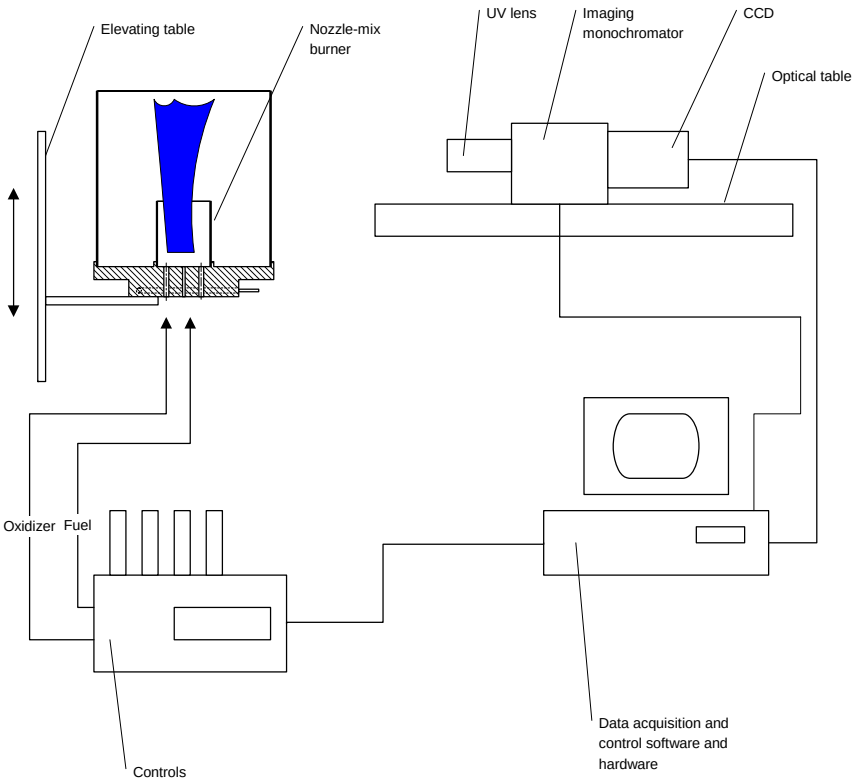


FIGURE 1. EXPERIMENTAL APPARATUS SCHEMATIC

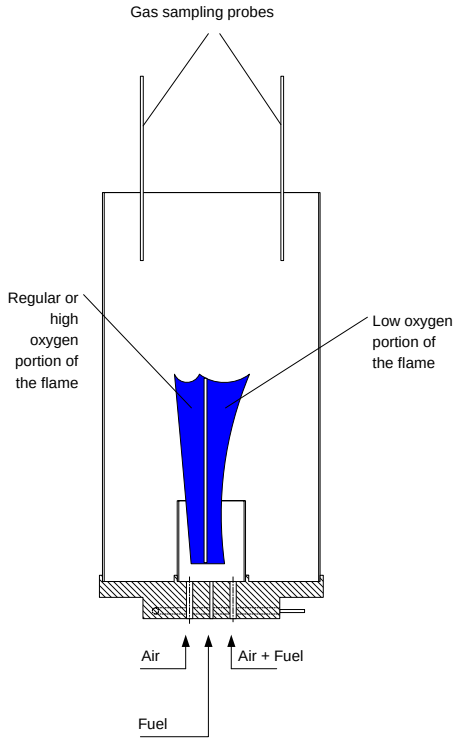


FIGURE 2. CONFIGURATION OF SOCS FOR HYBRID FLAME GENERATION

FIGURE 3 NOZZLE-MIXED BURNER, CONTROL SYSTEM, AND OPTICAL SENSOR

**Results and Analysis**

Typically, nozzle-mixed burners generate stable, low-$NO_x$, controllable flames. This type of burner has been widely used in various furnaces and other combustion equipment, including aluminum re-melt furnaces and glass-melting furnaces. In aluminum furnaces in particular, these burners are used to minimize dross formation in the melt.

Nozzle-mixed burners partially premix the oxidizer and fuel within the nozzle, causing the flame to have some attributes of both premixed and non-premixed combustion. The relative proportions depend on the degree of mixing achieved at the nozzle.[1] Therefore, the location and combustion characteristics of the conventional nozzle-mixed flame depend on how well the burner design is configured to produce the necessary mixing at the required rate. Even though combustion can be controlled by controlling the mixing process, the ability to control mixing and chemical processes in the burner is limited.

Normally, nozzle-mixed burners operate with 5-10% excess air to ensure complete combustion and prevent carbon monoxide emissions. This significant air excess results in a significant amount of oxygen in the flue gas. The major challenge in developing the new SOCS coupled with the low-dross Flex-Flame burner concept is to create combustion conditions where the fuel is completely oxidized, and the oxygen left in the flue gas is kept to the minimum possible concentration above the aluminum. Normally, combustion processes in nozzle-mixed flames are controlled by the rate of mixing of the fuel and oxidizer. To create a low-oxygen flue gas environment in the desired portion of the flame, small amounts of fuel were admixed to the right two air nozzles, leaving the left nozzles ejecting pure air into the mixing nozzle. The admixing of a small amount of fuel into the right-hand side oxidizer nozzles resulted in a new flame structure on the right side of the Flex-Flame burner.

[1] Turns, Stephen R., "An Introduction to Combustion: Concepts and Applications w/Software," 2000-01-01, McGraw-Hill Science/Engineering/Math.

Oxygen concentrations in the flue were measured at two locations; both at approximately 25 inches above the burner base (see Figure 4 Oxygen Concentrations in the Flue Gas with Varying Fuel Admixing for 5% Excess Air). The purpose of these measurements was to use conventional combustion gas analyses techniques to determine if a low-oxygen-flue-gas zone could be created without affecting the burner's efficiency and emissions characteristics. Experiments showed that adding a small amount of fuel to the right side air nozzles with the same reduction of fuel flow rate in the main fuel port resulted in a redistribution of the "left-over" oxygen concentration profile in the flue gas. Figures 4(a) and 4(b) show that the oxidizing atmosphere of the flue gas can be controlled by admixing fuel to one side of the flame. For both 5% and 10% excess air, this effect becomes apparent when slightly more than 1 L/min of fuel, out of the 15 L/min of fuel in the central jet, is admixed. For both excess air levels, admixing 3 L/min of fuel reduced the concentration of oxygen in the flue gas, on the same side, by about

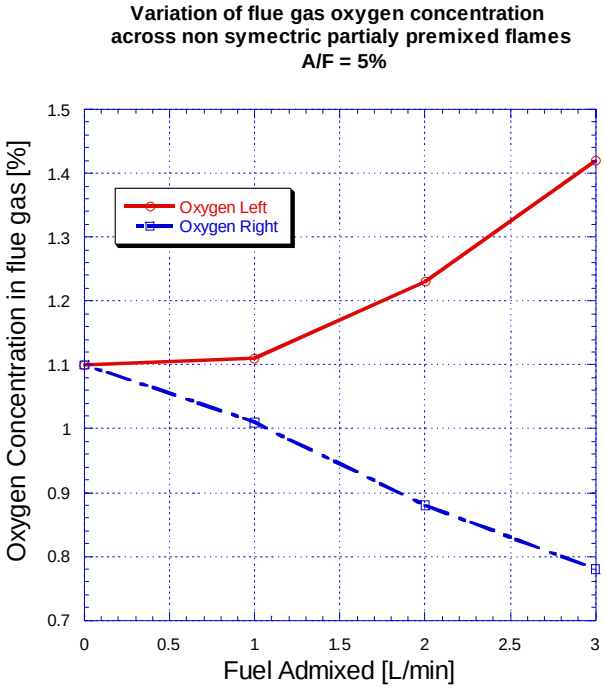


FIGURE 4 OXYGEN CONCENTRATIONS IN THE FLUE GAS WITH VARYING FUEL ADMIXING FOR 5% EXCESS AIR

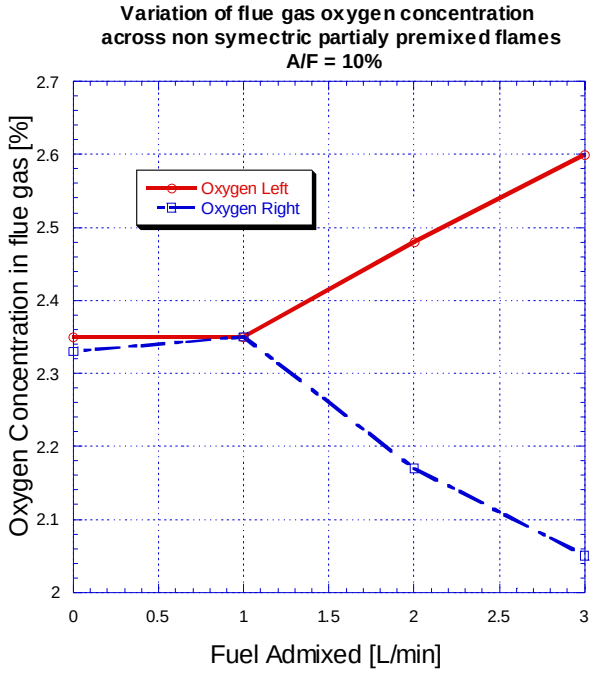


FIGURE 5 OXYGEN CONCENTRATIONS IN THE FLUE GAS WITH VARYING FUEL ADMIXING FOR 10% EXCESS AIR

Figure 6 Spectra Acquired from Nozzle-Mix Burner Flamesportrays the technique by which the nozzle-mix burners were analyzed with the spectrometer-CCD system. Because spectrometers are only imaging in one dimension, cross-sections of the flame were analyzed spectrally at several locations within the flame. Using this technique all sub-radicals emitting light can be viewed at several locations within the flame. This data can be used to reconstruct a map of the desired emission radicals through data processing.

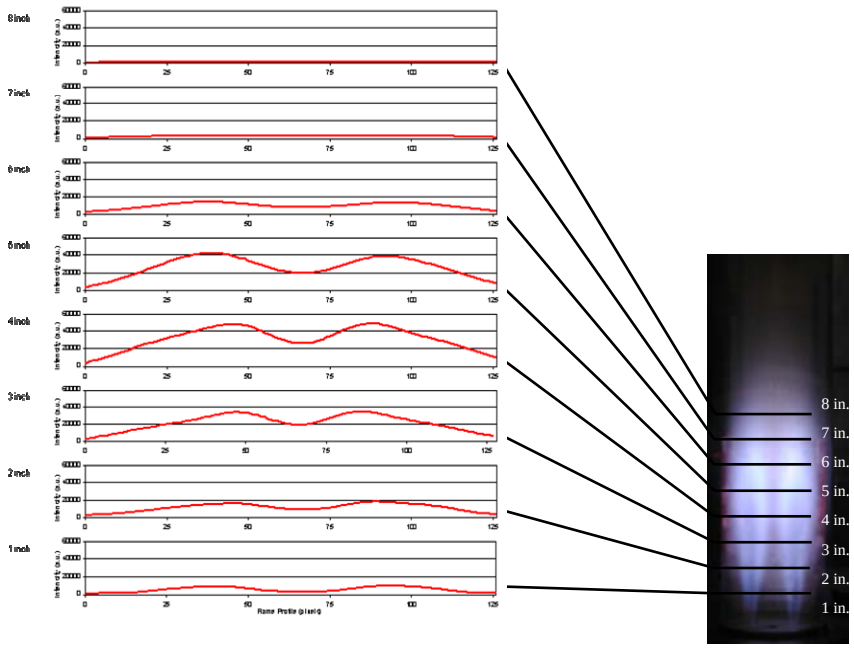


FIGURE 6 SPECTRA ACQUIRED FROM NOZZLE-MIX BURNER FLAMES

Nozzle-mix burner flames were found to show OH* and CH* emission intensities that first increase with the flame direction until they maximize in the upper half of the flames. The emission peaks of CH radicals (CH*) are lower than the OH* peaks in the spectra at any location along the flame. The concentration of the CH radicals in a 43%EA lean flame were found to be low because of carbon oxidation to CO and, finally, to $CO_2$ in the abundance of oxygen and oxidizing radicals (for example OH*). $I_{OH}/I_{CH}$ ratio values measured in rich flames (for examples 0%EA) are lower than those measured for leaner flames.

In order to determine whether the flame spectra change when flame shape is varied, asymmetric flames were generated with the nozzle-mix burner by 'admixing' a small amount of fuel to the oxidizer nozzles on one side of the flame. The admixing of a small amount of fuel into the right-hand-side oxidizer's nozzles resulted in spectrally observable changes to the flame.

Figure 8 and Figure 9 show significant increases in OH radical emission in the right portion of the flame relative to no fuel admixing, which is depicted in

Figure 7. Concurrently CH* emission profiles did not change in both right and left portions of the flames. Spectroscopic measurements show the existence of an additional strong source of OH* emission. Therefore, the presence of new OH* emission enhancement can be explained by the presence of a new premixed flame formation existing at approximately the same location as the conventional nozzle-mixed flame structure. This fact can be explained by the creation of a new turbulent double flame structure.

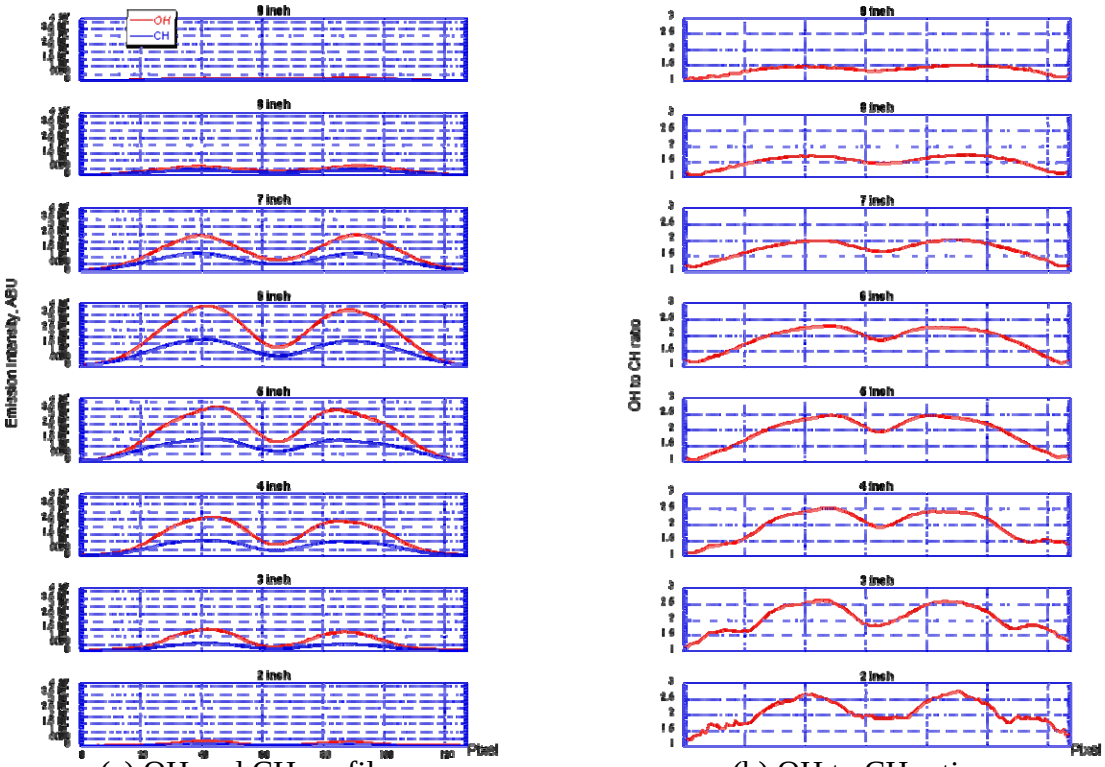


(a) OH and CH profiles (b) OH to CH ratio

FIGURE 7 0 L/M FUEL ADMIXING ON RIGHT; 5%EA; FUEL: 15 L/M; AIR: 154 L/M

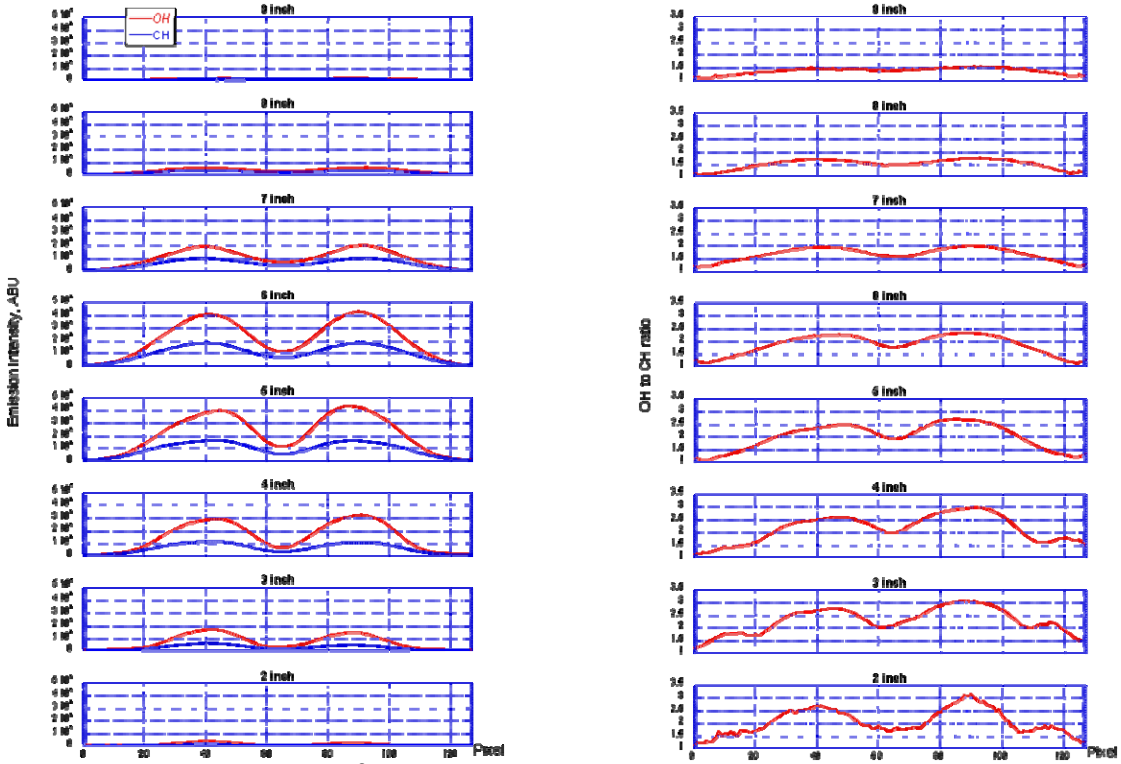


(a) OH and CH profiles (b) OH to CH ratio

FIGURE 8 1 L/M FUEL ADMIXING ON RIGHT; 5%EA; FUEL: 14 L/M; AIR: 154 L/M

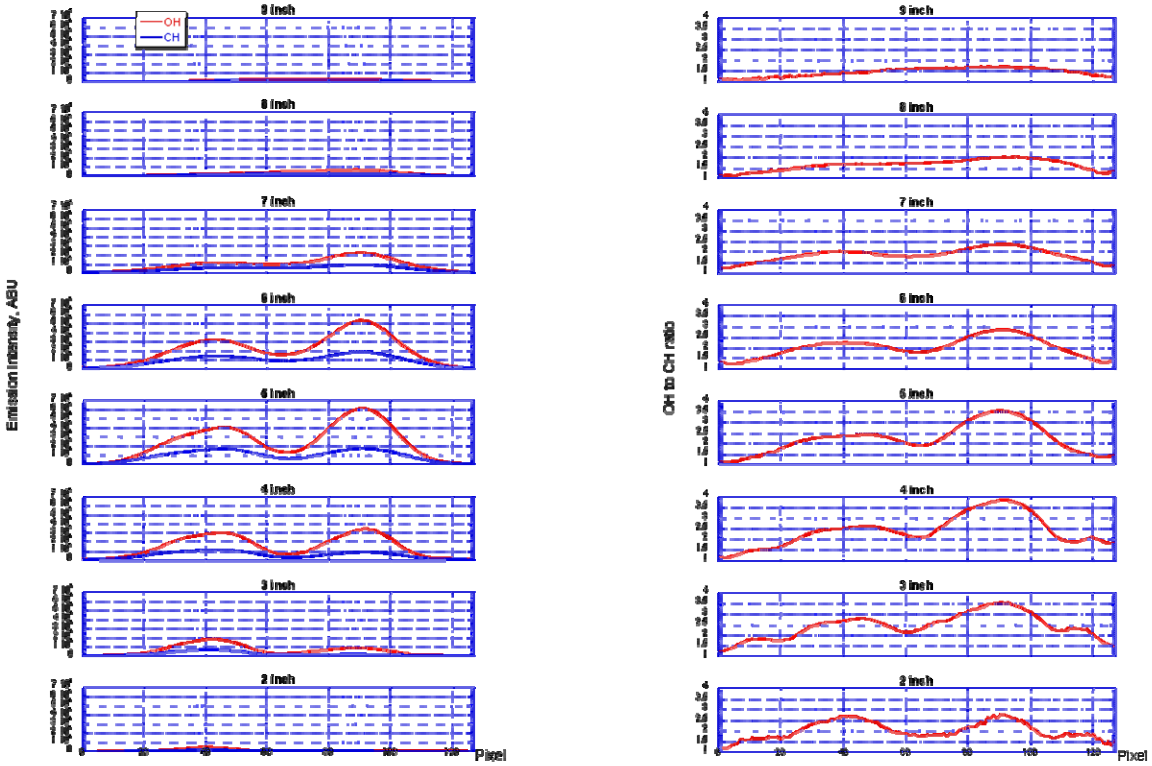


(a) OH and CH profiles (b) OH to CH ratio

FIGURE 9 2 L/M FUEL ADMIXING ON RIGHT; 5%EA; FUEL: 13 L/M; AIR: 154 L/M

**WORK COMPLETED IN PHASE I, TASKS 5-9**

**Experimental Arrangements**

After completing the laboratory scale SOCS or Flex-Flame burner, the SOCS concept was further studied on a pilot-scale 0.8 to 1.0 MMBtu/hr burner system. A photograph of this burner set-up is shown in Figure 10.

The mounted burner and the flow control skid are shown. This burner is flexible enough to handle firing rates up to 1 MMBtu/h, operate over a wide range of air/fuel ratios, allow separate air flow to the four internal nozzles, and allow admixing of fuel and air.

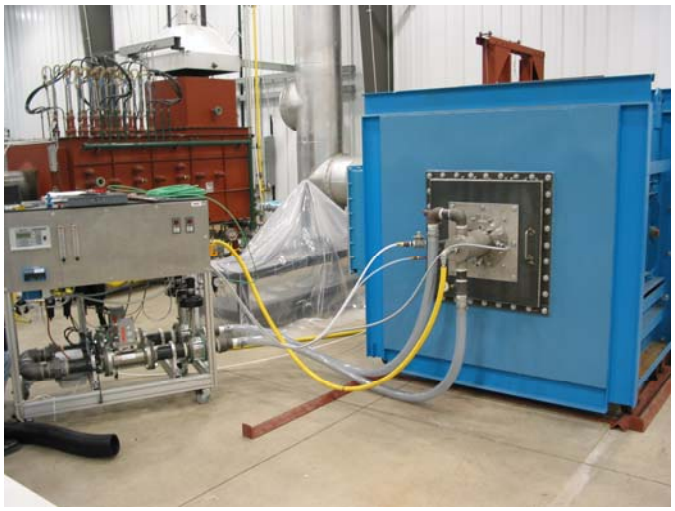

FIGURE 10 SOCS/FLEX-FLAME BURNER MOUNTED ON FURNACE AND CONNECTED TO AIR/GAS DELIVERY SKID

Figure 11 is a diagram of the 1.0 MMBtu/h nozzle-mixed burner used for pilot-scale testing. The burner has a central fuel jet surrounded by eight air jets. Secondary air can be introduced above the primary air jets.

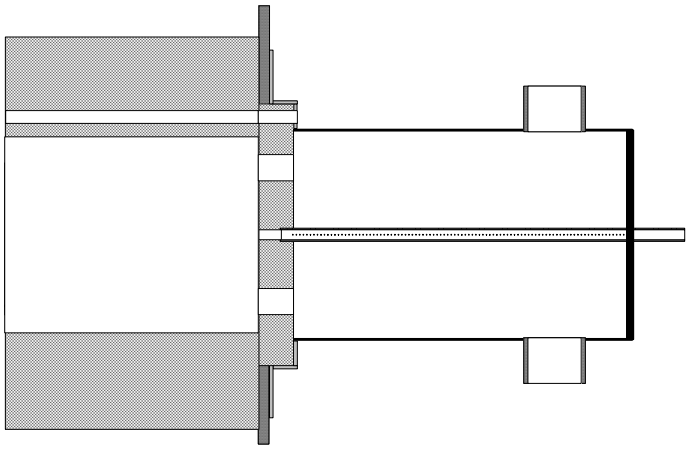

FIGURE 11 NOZZLE-MIXED 1 MMBTU/HR BURNER

This burner consists of two separate chambers in the vertical direction. This configuration allows for two separate flows of main combustion air to be metered and controlled. The 8 air nozzles are aligned on a circle 3.5 inches in diameter around the main fuel nozzle. Secondary fuel can be admixed to either combustion air chamber, so that the flame can be partially premixed. Secondary air can also be introduced directly to the upper portion of the flame inside the furnace via 3 openings in the burner block, as shown in Figure 11. Five water-cooled sampling probes were inserted at the locations in the furnace shown in Figure 12. These probes were left inside the furnace throughout the duration of each test. Each probe can acquire temperatures and gas samples to be sent to the analyzer. Probes 1 and 2 draw samples directly above the flame and can provide information about the progression of combustion along the length of the flame.

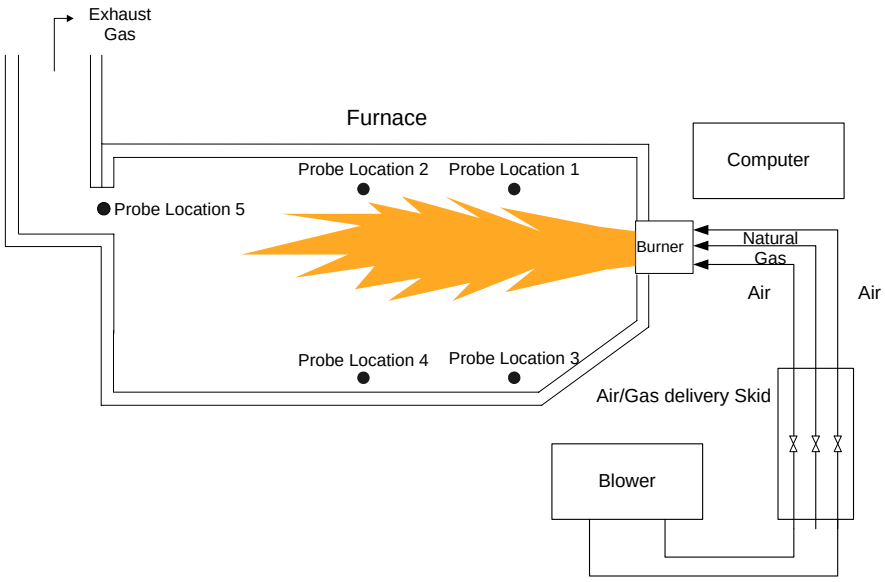


FIGURE 12 FURNACE AND SAMPLING PROBE LOCATIONS

Probes 3 and 4 drew samples from 2 inches above the hearth and can give good estimates of the concentration profile directly above the furnace floor. Probe 5 sampled the furnace exhaust and provided information about flue gas composition after good mixing has occurred. In addition to the five thermocouples inside the probes, there were six more thermocouples permanently installed on the roof of the furnace. They penetrate the insulation and measure temperatures 1/2 inch above the furnace ceiling. These thermocouples were used to monitor the refractory temperature profile and assure that steady-state temperature has been achieved prior to testing.

**Air/Gas Delivery Skid**

The air/gas delivery skid is a portable system, designed to meet the requirements of any burner that has multiple air and natural gas flows. Specifically, it can control and meter the following flows:

1. Two independent air flows from the blower, measuring up to 5300 liters/minute each.
2. Two natural gas flows at 760 liters/minute (main fuel flow, corresponding to 1 MMBtu/hr) and 76 liters/minute (secondary fuel flow, corresponding to 100,000 Btu/hr).
3. One secondary air flow at 1000 liters/minute.
4. Pilot air and pilot natural gas flows.

In addition, the air/gas delivery skid has a built-in analog temperature acquisition platform for up to 18 thermocouples of any type. The skid also has a flame management/safety system for the main and pilot flames.

**Computer/Analyzer**

A laptop computer was used to monitor and record all temperatures and emission levels during the tests. The data-acquisition program installed on this computer can communicate with the temperature input modules that are located on the skid. Emissions measurements from the analyzer are also monitored and

recorded. The analyzer is a compact portable device that rests on top of the air/gas delivery skid and can measure $O_2$, $CO_2$, CO, $NO_X$, and $SO_2$.

**Experimental Procedure and Results**

The furnace was allowed to warm up for 2 hours prior to each test. It was established that 2 hours is adequate warm-up time to obtain an average steady-state temperature of approximately 2000°F at the six thermocouples inside the furnace roof refractory. Steady-state temperatures inside the furnace are needed to achieve reproducible results. After the completion of the warm-up period, each change in firing conditions, whether fuel admixing or introducing secondary air, was accompanied by 30 minutes of data acquisition. Of those 30 minutes, the first five minutes were intended for stabilization and were not considered as steady-state data. The remaining time was spent recording emissions and temperatures. At the end of each test, the data acquired over the 25 minutes were averaged and a single value representing that state was used as the result. Using this method, the effects of random spikes in temperature or concentration were suppressed.

The experiments examined the impact of the two methods: fuel doping and introduction of secondary air to the main combustion zone. In the fuel-doping cases, certain percentages of fuel were subtracted from the main fuel flow and admixed to the lower burner chamber. The reasoning behind the fuel-doping method is that the lower portion of the flame will become more fuel-rich than the upper portion; thus creating a hybrid flame. For the secondary air introduction tests, predetermined percentages of air were subtracted from the upper and lower burner chambers in equal amounts and were introduced directly into the upper part of the flame for a second-stage burn.

Figure 13, Figure 14, and Figure 15, illustrate the results obtained from fuel doping into the lower burner chamber and introducing secondary air to the upper part of the flame. These figures show that doping up to 12% of the total fuel into the lower half of the burner had little impact on CO, $NO_x$, and $O_2$ concentrations above the flame, along the furnace hearth, or in the exhaust. The sample probes were numbered, as shown in Figure 7, and are:

- Probes 1 and 2 - above the flame.
- Probes 3 and 4 - along the furnace hearth (below the flame).
- Probe 5 - the furnace exhaust.

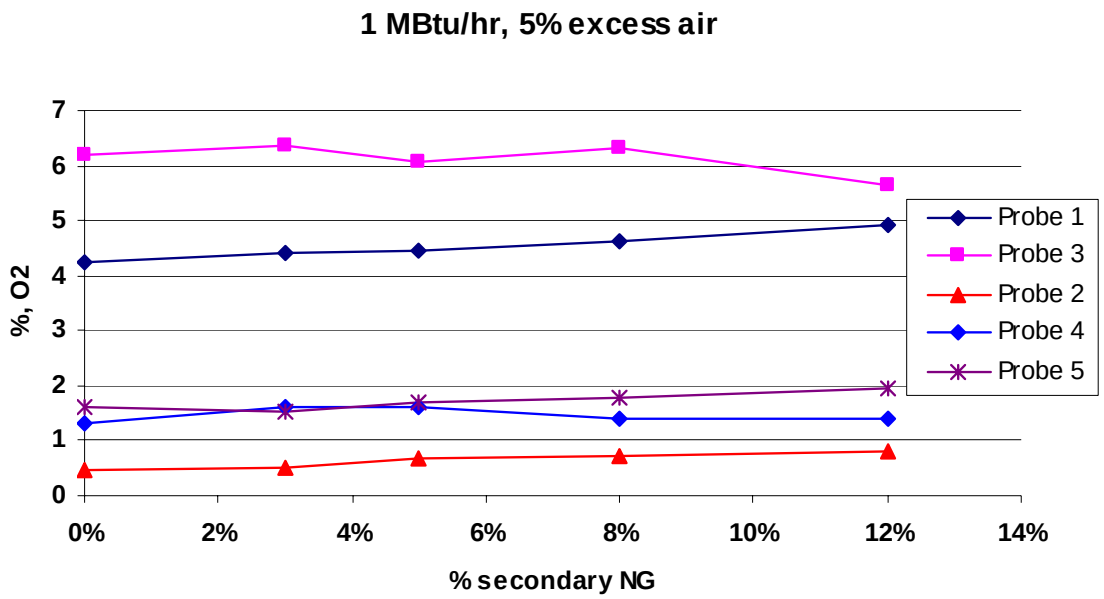


FIGURE 13 OXYGEN CONCENTRATIONS WITH NATURAL GAS DOPING

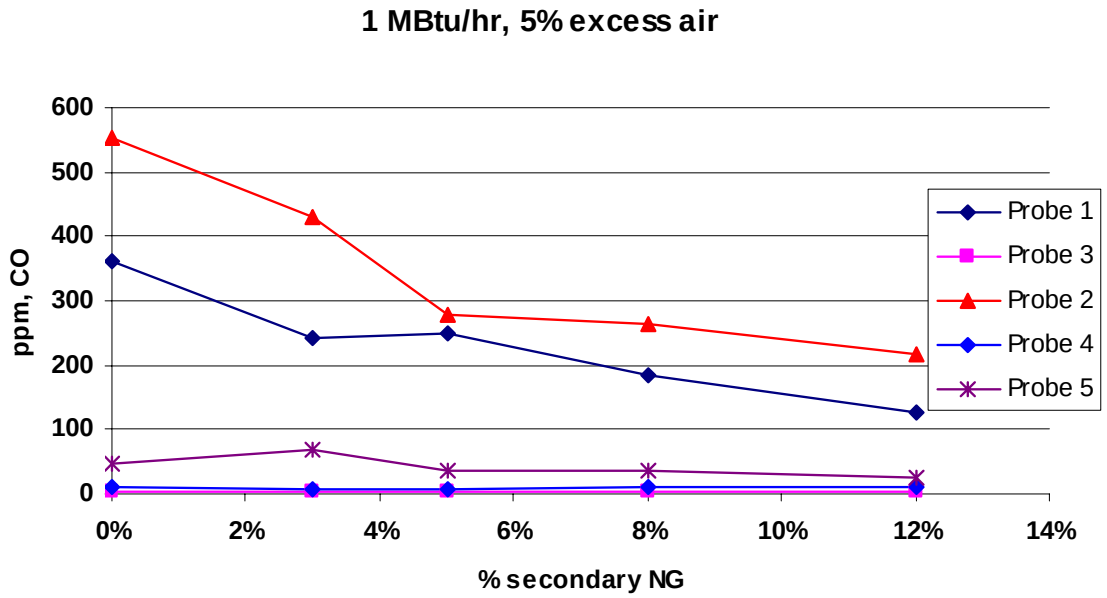


FIGURE 14 CARBON MONOXIDE CONCENTRATIONS WITH NATURAL GAS DOPING

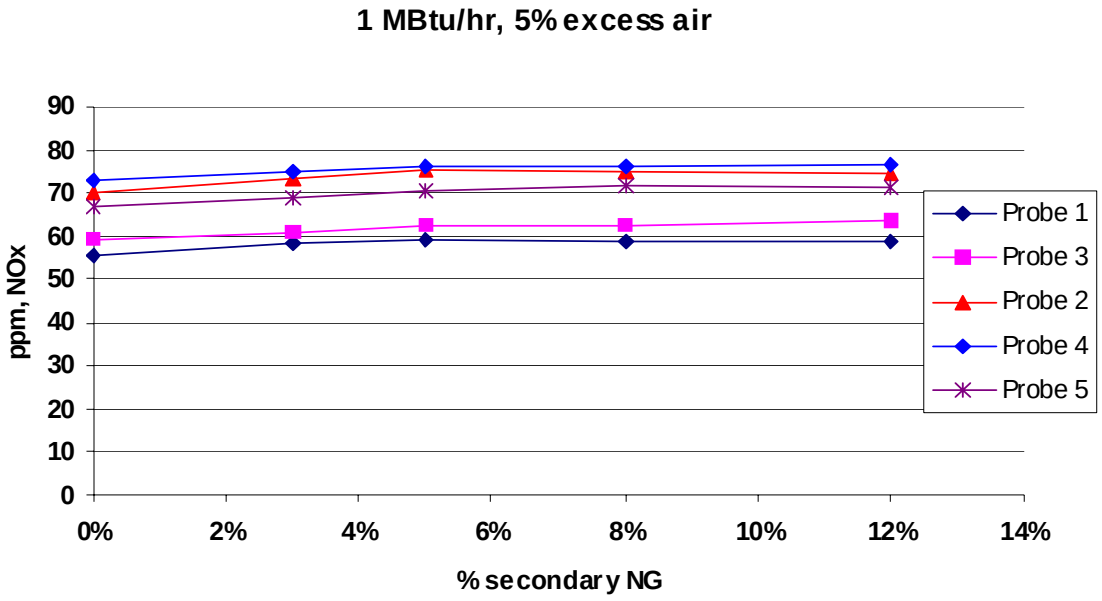


FIGURE 15 $NO_X$ CONCENTRATIONS WITH NATURAL GAS DOPING

The second approach to create fuel-lean-top / low-oxygen-bottom flames was the "secondary air method". In these tests, the air flow to the primary jets of the SOCS/Flex-Flame burner was reduced by 5-20%. Concurrently, and in order to keep the overall air/fuel ratio constant, an identical amount of air was injected directly to the furnace through the "secondary air" ports in the burner block shown in Figure 6.

Figure 16, Figure 17, and Figure 18 illustrate the results obtained from introducing secondary air to the upper part of the flame. The five sampling probe locations were the same as in the fuel-doping tests. Oxygen and carbon monoxide were unchanged in the exhaust, while $NO_x$ was reduced by 15 to 20 percent. Along the length of the flame, the secondary air injection dramatically changed the concentrations of oxygen and carbon dioxide above and below the flame. As more secondary air was injected above the flame, the oxygen content above the flame increased while the oxygen content below the flame decreased. The reverse effect, as expected, was seen for carbon dioxide. The largest impact was seen for 15-20% secondary air injection above the flame. In these cases, oxygen concentration below the flame was reduced by approximately 35%.

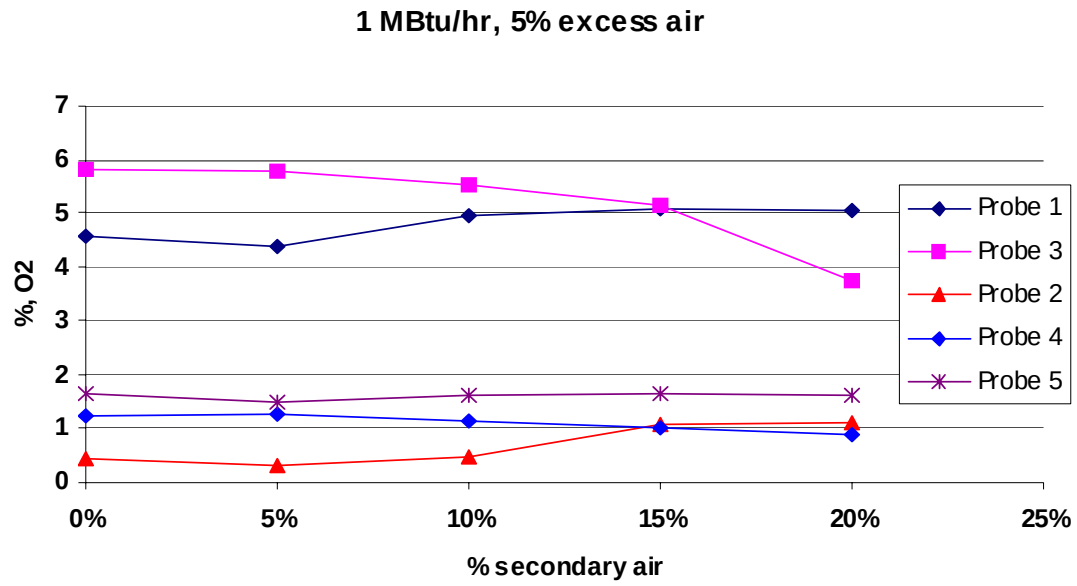


FIGURE 16 OXYGEN CONCENTRATIONS WITH SECONDARY AIR INJECTION

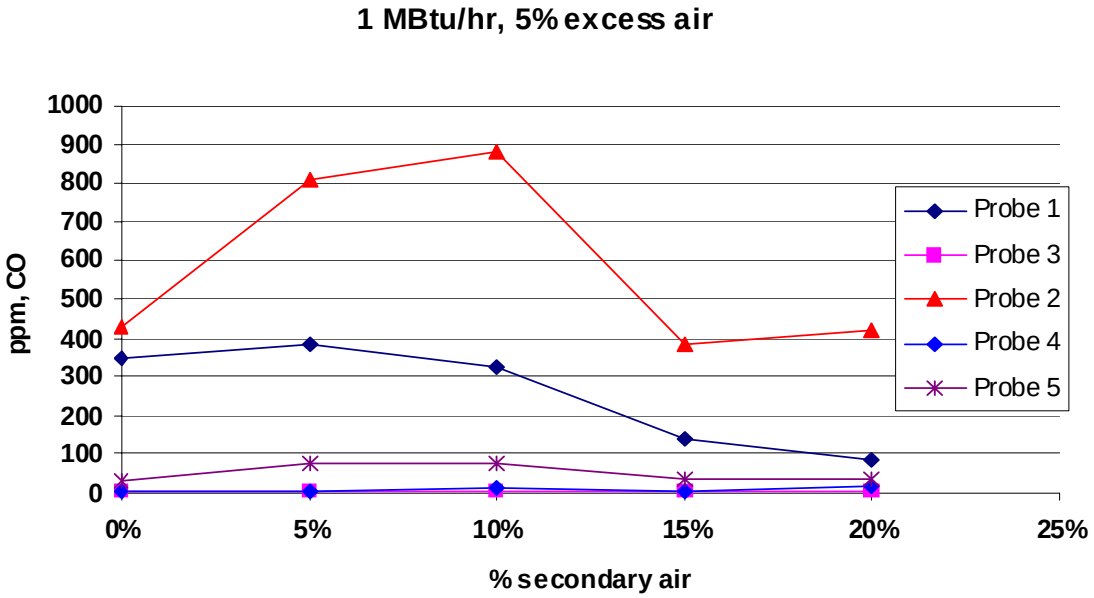


FIGURE 17 CARBON MONOXIDE CONCENTRATIONS WITH SECONDARY AIR INJECTION

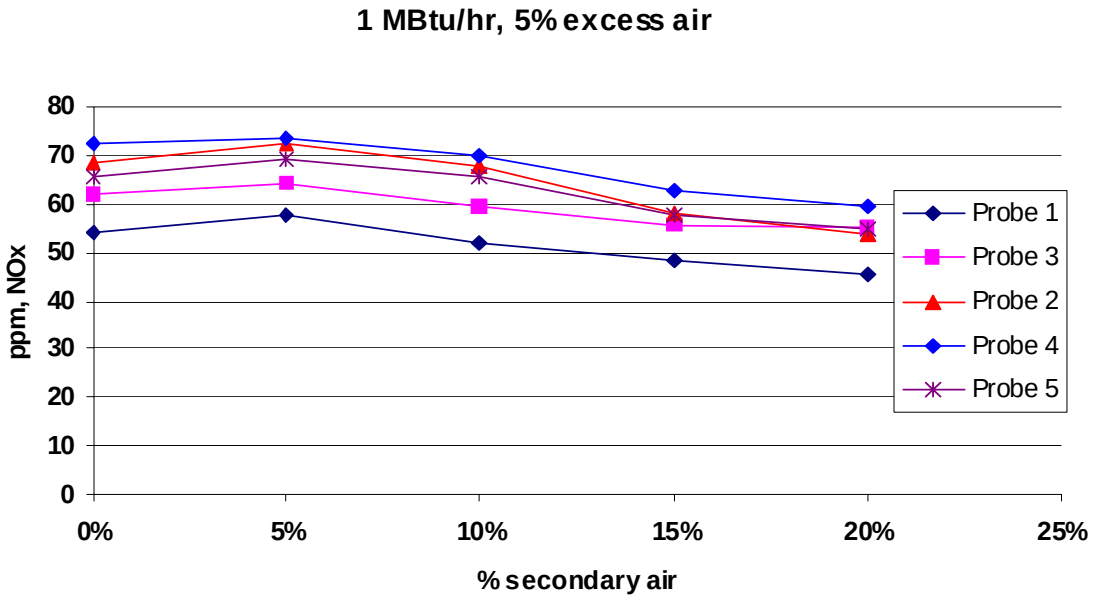


FIGURE 18 $NO_X$ CONCENTRATIONS WITH SECONDARY AIR INJECTION

**Results Analysis and Discussion**

Pilot-scale burner tests with fuel doping did not produce a significant decrease in oxygen concentration above the furnace hearth. This could be the result of strong mixing of the air/fuel flows inside the burner block. Even though the fuel was admixed to the lower burner chamber, the high velocities of the air and gas streams inside the burner block could have mixed the two air streams with the natural gas stream to such an extent that the resulting flame had a uniform distribution of intermediate combustion species.

The introduction of secondary air, however, produced results that are more positive. As the graphs demonstrate, there is a decrease in oxygen concentration of about 40%, sampled 2 inches above the furnace hearth. The overall oxygen level at the exhaust does not exhibit any significant change for any of the excess air cases, and, thus, the overall combustion efficiency remains unaffected. Furthermore, for all probe locations, when the secondary air was introduced to the flame, the $NO_x$ values steadily decreased and reached levels 15-20% lower than the baseline case.

**Commercial Burner (1 MMBtu/hr total firing rate)**

Based on the findings from the prototype 0.8 - 1 MMBtu/hour nozzle-mix burner, a commercial burner, the, Eclipse® Combustion ThermJet burner was selected for further pilot-scale testing. This industrially accepted high-momentum burner is widely used in aluminum melting. This burner is further explained and described in the next section. Since the fuel-doping method did not yield positive results on the nozzle-mix burner, only the secondary air variations were studied with the ThermJet burner. For the tests, the burner was modified to allow secondary air to be introduced at the top of the burner.

The testing of the prototype 1 MMBtu/hour medium-momentum burner showed that introducing secondary air above the main flame can reduce oxygen concentration near the furnace hearth and $NO_x$ emissions from the furnace. Lower oxygen concentrations near the aluminum melt would signify an

accompanying decrease in the formation of dross compared to the furnaces currently used for aluminum melting. In industry, however, high-momentum burners are commonly used, rather than the medium-momentum nozzle-mix prototype burner described above. For this reason, a 1-MMBtu high-momentum ThermJet burner, manufactured by Eclipse Combustion, was purchased and modified for testing. The ThermJet is an industrially accepted burner system and is thoroughly proven.

**Test Burner Configuration**

Figure 19 shows the ThermJet burner. It produces a high-momentum flame with a flame jet velocity of approximately 500 ft/sec, approximately twice the jet velocity of the prototype burner. This burner was selected because most aluminum melting facilities desire the enhanced convective heat transfer that high-momentum burners, such as the ThermJet, offer.

The only modification to this burner was a nozzle that introduced secondary air directly above the flame (Figure 20). This secondary air stream enabled burner operation slightly below stoichiometric air levels to provide low oxygen concentrations directly above the aluminum melt, while maintaining overall stoichiometry.

FIGURE 19. STANDARD THERMJET BURNER

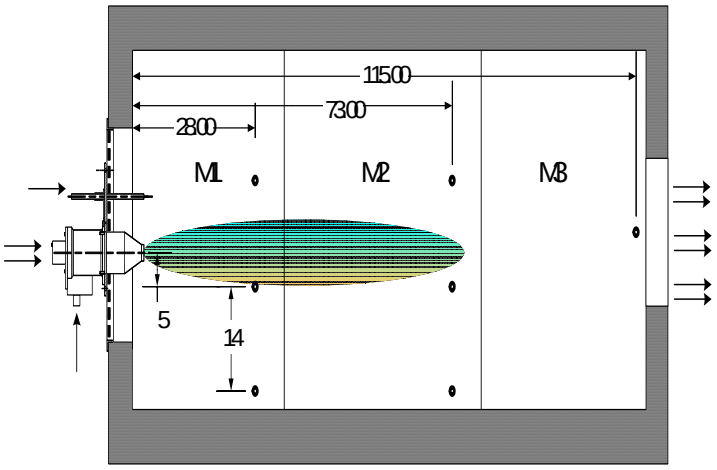


FIGURE 20 MODIFIED THERMJET BURNER

The secondary air line's angle of entry with respect to the flame was variable to allow tests to determine the optimum angle for introducing secondary air to the furnace chamber. Four angles were tested: 0°, 5°, 10°, and 15°, all pointing away from the flame to postpone mixing of the secondary air stream with the main flame.

Another feature of the secondary air line was its exit nozzle size. Two nozzle diameters were used to allow for different air velocities. The graphs in the next section categorize the secondary air flow as “high-velocity” (5 mm exit nozzle diameter) or “low-velocity” (10 mm exit nozzle diameter).

The number of sampling probes in the furnace was increased to seven: three in furnace module 1 (M1), three in module 2, (M2) and one in the exhaust zone (M3) (Figure 21).

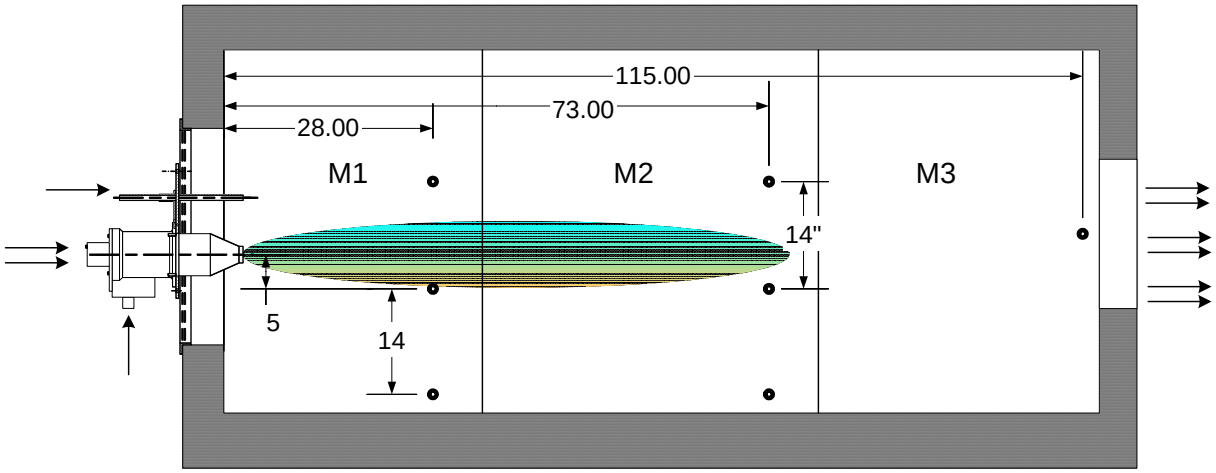


FIGURE 21 FURNACE SCHEMATIC AND PROBE LOCATIONS FOR THERMJET BURNER TESTS
(ALL DIMENSIONS ARE IN INCHES. FURNACE INTERIOR WIDTH IS APPROXIMATELY 60 INCHES.)

**Results**

Figure 22 shows the effect in the first furnace module of introducing low-velocity secondary air above the flame at 0°. While the oxygen concentration at the exhaust remained approximately the same with increasing secondary air injection, the oxygen concentration two inches above the hearth decreased to approximately 20% below baseline.

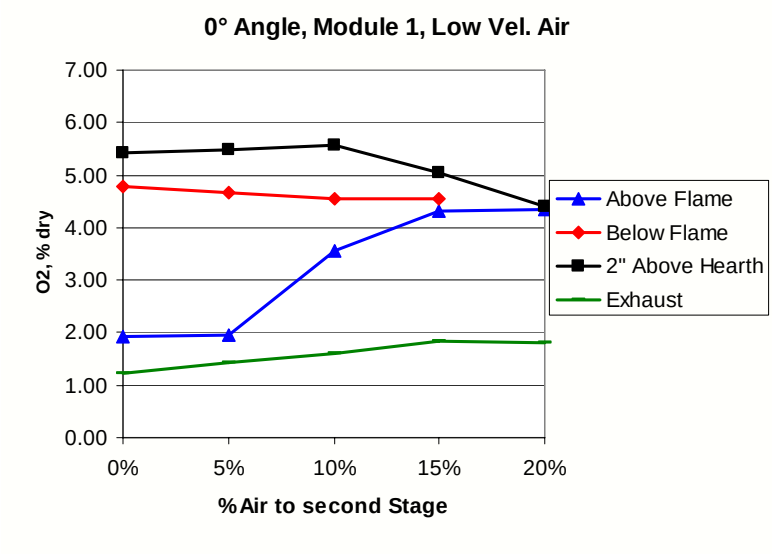


FIGURE 22 EFFECT IN MODULE 1 OF LOW-VELOCITY SECONDARY AIR INJECTION AT 0º FROM THE THERMJET BURNER

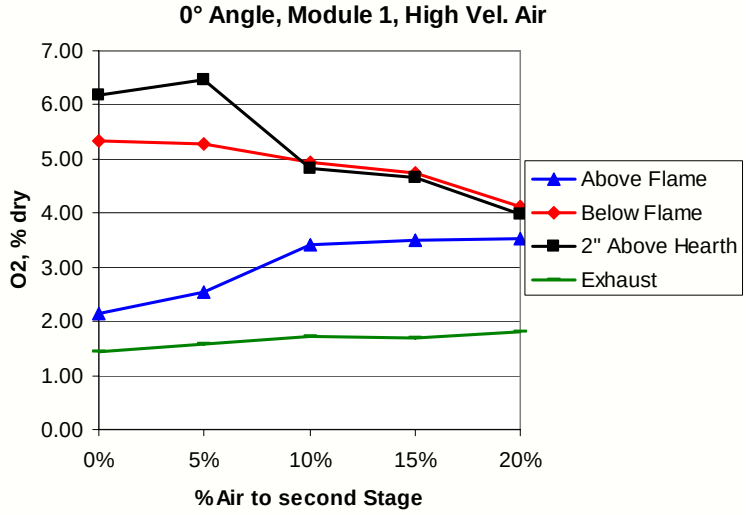


FIGURE 23 EFFECT IN MODULE 1 OF HIGH-VELOCITY SECONDARY AIR INJECTION AT 0º FROM THE THERMJET BURNER

Figure 23 shows the effect in the first furnace module of introducing high-velocity secondary air above the flame at 0°. While the oxygen concentration at the exhaust remained approximately the same with increasing secondary air injection, the oxygen concentration two inches above the hearth showed an even greater decrease than with the low-velocity air injection (to approximately 35% below baseline)

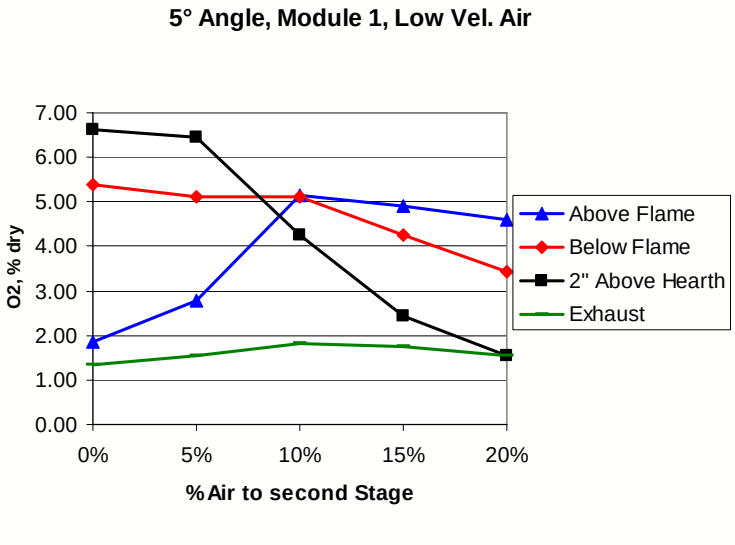


FIGURE 24 EFFECT IN MODULE 1 OF LOW-VELOCITY SECONDARY AIR INJECTION AT 5º AWAY FROM THE THERMJET BURNER

Figure 24 shows the effect in the first furnace module of introducing low-velocity secondary air above the flame at 5°. While the oxygen concentration at the exhaust remained approximately the same with increasing secondary air injection, the oxygen concentration two inches above the hearth decreased to approximately 78% below baseline.

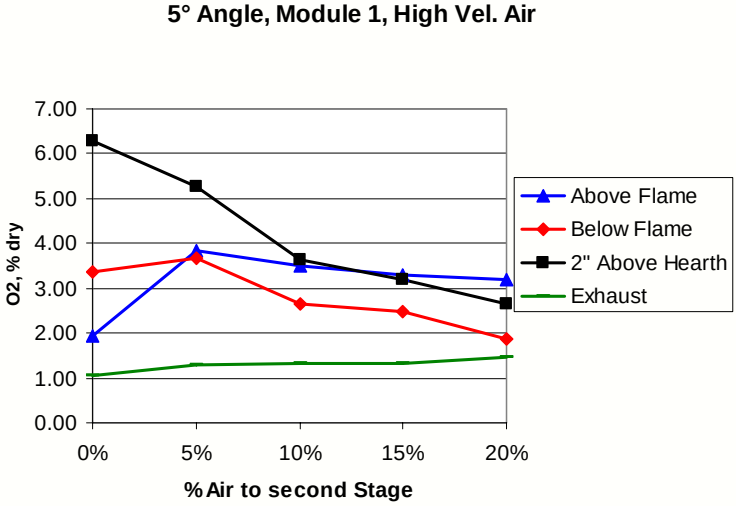


FIGURE 25 EFFECT IN MODULE 1 OF HIGH-VELOCITY SECONDARY AIR INJECTION AT 5º AWAY FROM THE THERMJET BURNER

Figure 25 shows the effect in the first furnace module of introducing high-velocity secondary air above the flame at 5°. While the oxygen concentration at the exhaust remained approximately constant with increasing secondary air injection, the oxygen concentration two inches above the hearth decreased to approximately 55% below baseline.

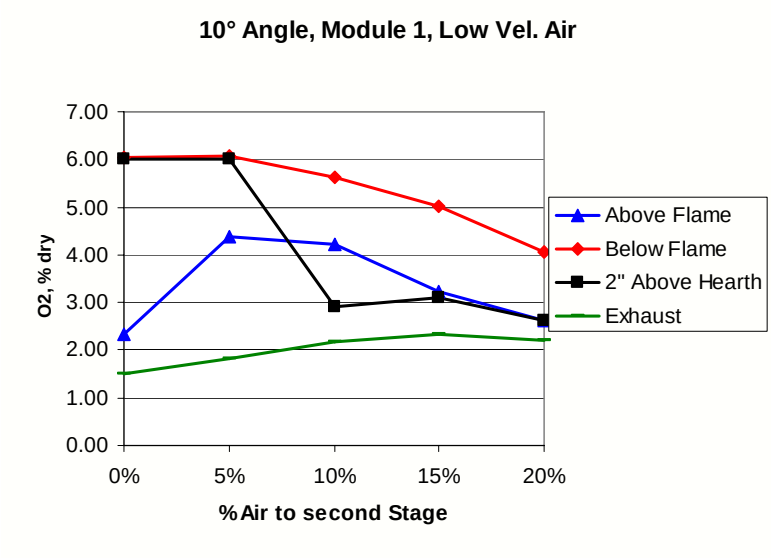


FIGURE 26 EFFECT IN MODULE 1 OF LOW-VELOCITY SECONDARY AIR INJECTION AT 10º AWAY FROM THE THERMJET BURNER

Figure 26 shows the effect in the first furnace module of introducing low-velocity secondary air above the flame at 10°. While the oxygen concentration at the exhaust remained approximately constant with increasing secondary air injection, the oxygen concentration two inches above the hearth decreased to approximately 58% below baseline.

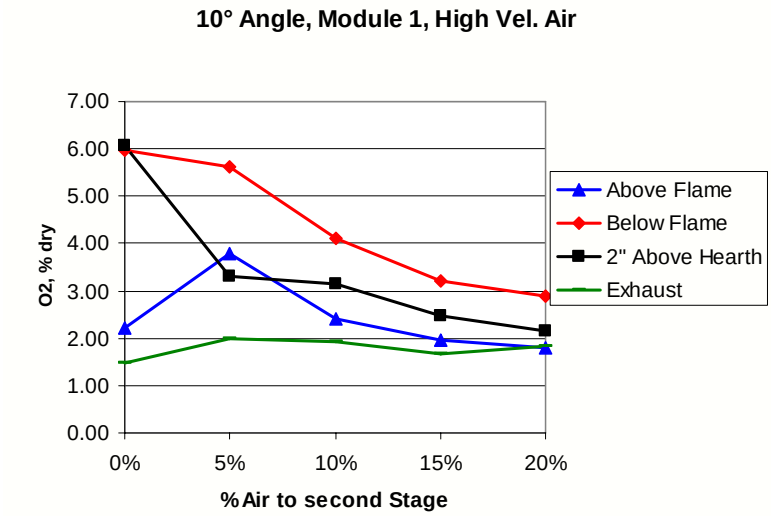


FIGURE 27 EFFECT IN MODULE 1 OF HIGH-VELOCITY SECONDARY AIR INJECTION AT 10º AWAY FROM THE THERMJET BURNER

Figure 27 shows the effect in the first furnace module of introducing high-velocity secondary air above the flame at 10°. While the oxygen concentration at the exhaust remained approximately the same with increasing secondary air injection, the oxygen concentration two inches above the hearth decreased to approximately 65% below baseline.

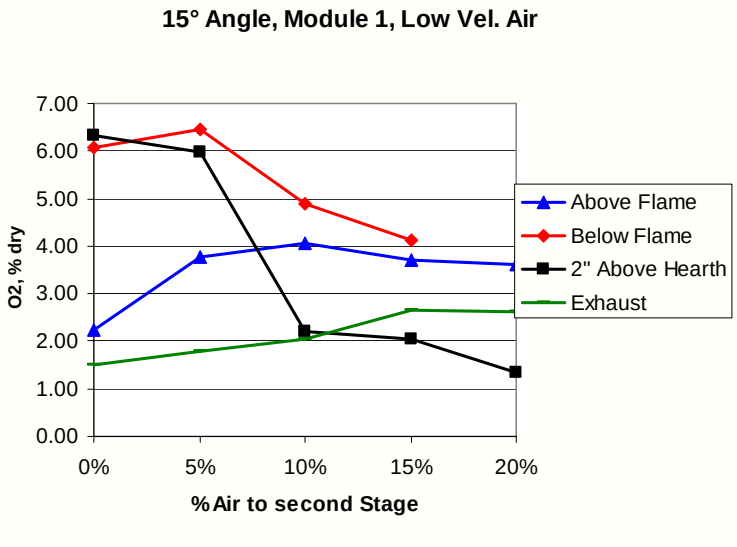


FIGURE 28 EFFECT IN MODULE 1 OF LOW-VELOCITY SECONDARY AIR INJECTION AT 15º AWAY FROM THE THERMJET BURNER

Figure 23 shows the effect in the first furnace module of introducing low-velocity secondary air above the flame at 15°. While the oxygen concentration at the exhaust remained approximately constant with increasing secondary air injection, the oxygen concentration two inches above the hearth decreased to approximately 79% below baseline.

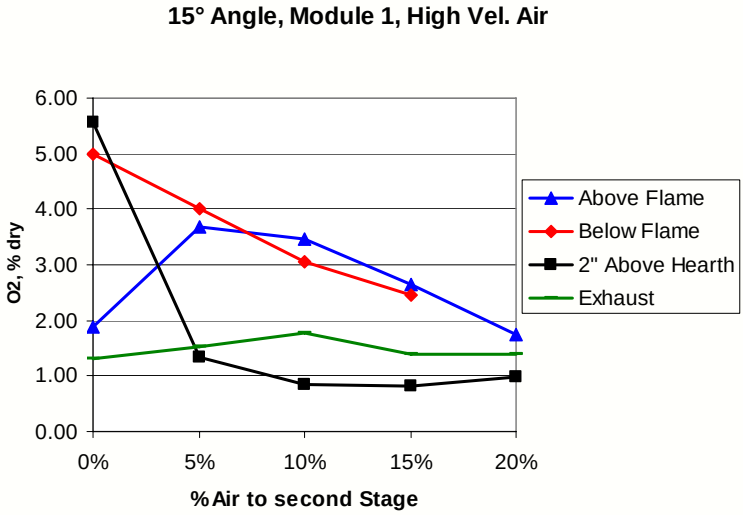


FIGURE 29 EFFECT IN MODULE 1 OF HIGH-VELOCITY SECONDARY AIR INJECTION AT 15º AWAY FROM THE THERMJET BURNER

Figure 30 shows the effect in the first furnace module of introducing high-velocity secondary air above the flame at 15°. While the oxygen concentration at the exhaust remained approximately the same with increasing secondary air injection, the oxygen concentration two inches above the hearth decreased to approximately 82% below baseline.

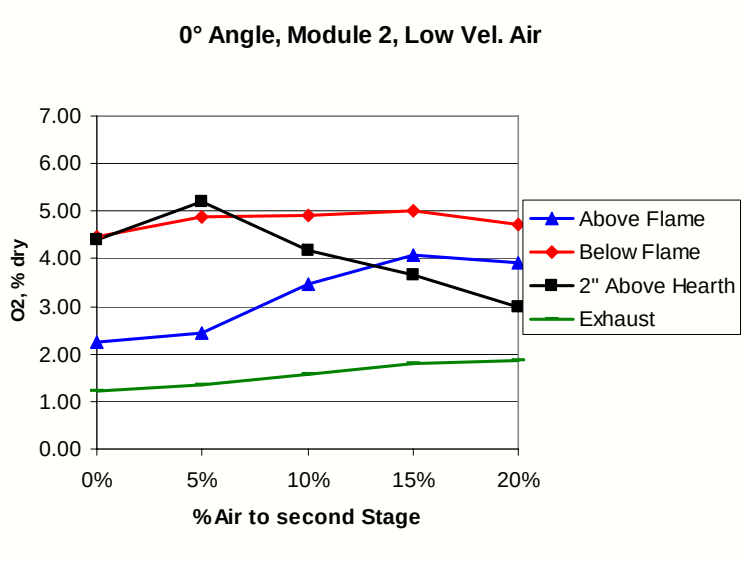


FIGURE 30 EFFECT IN MODULE 2 OF LOW-VELOCITY SECONDARY AIR INJECTION AT 0º FROM THE THERMJET BURNER

Figure 30 shows the effect in the second furnace module of introducing low-velocity secondary air above the flame at 0°. While the oxygen concentration at the exhaust remained approximately the same with increasing secondary air injection, the oxygen concentration two inches above the hearth decreased to approximately 30% below baseline.

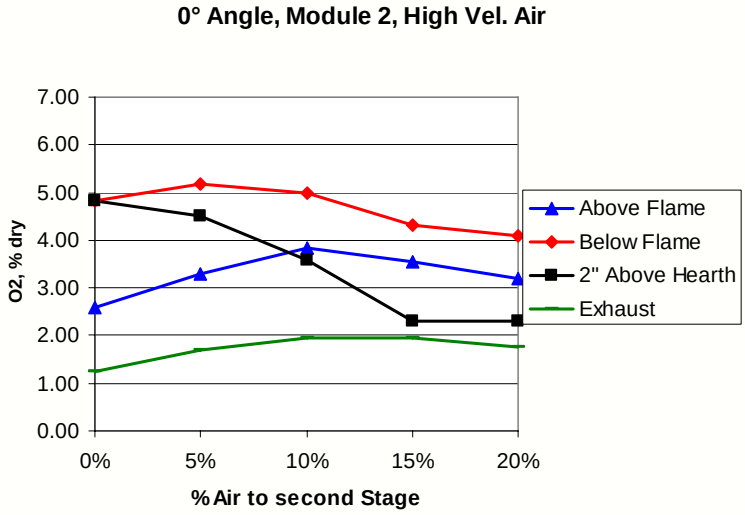


FIGURE 31 EFFECT IN MODULE 2 OF HIGH-VELOCITY SECONDARY AIR INJECTION AT 0º FROM THE THERMJET BURNER

Figure 31shows the effect in the second furnace module of introducing high-velocity secondary air above the flame at 0°. While the oxygen concentration at the exhaust remained approximately the same with increasing secondary air injection, the oxygen concentration two inches above the hearth decreased to approximately 55% below baseline.

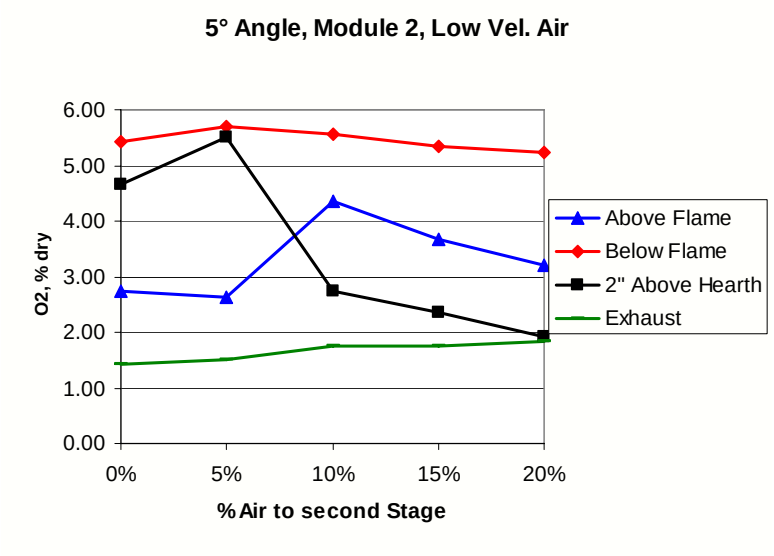


FIGURE 32 EFFECT IN MODULE 2 OF LOW-VELOCITY SECONDARY AIR INJECTION AT 5º AWAY FROM THE THERMJET BURNER

Figure 32 shows the effect in the second furnace module of introducing low-velocity secondary air above the flame at 5°. While the oxygen concentration at the exhaust remained approximately the same with increasing secondary air injection, the oxygen concentration two inches above the hearth decreased to approximately 56% below baseline.

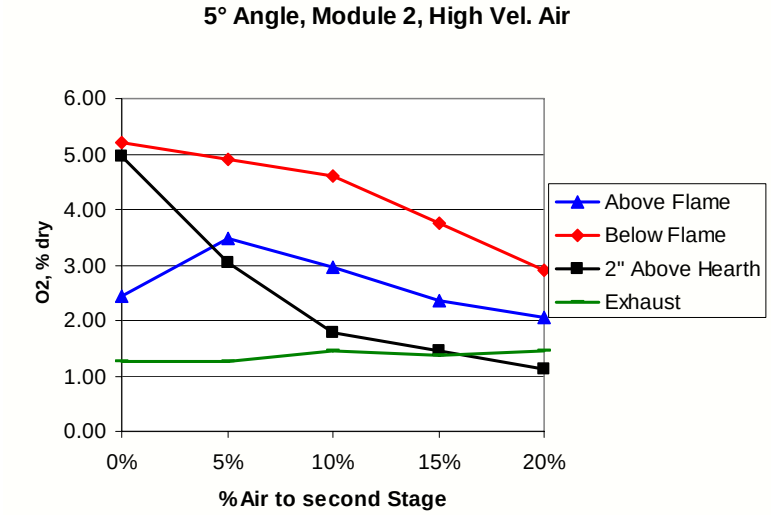


FIGURE 33 EFFECT IN MODULE 2 OF HIGH-VELOCITY SECONDARY AIR INJECTION AT 5º AWAY FROM THE THERMJET BURNER

Figure 33 shows the effect in the second furnace module of introducing high-velocity secondary air above the flame at 5°. While the oxygen concentration at the exhaust remained approximately the same with increasing secondary air injection, the oxygen concentration two inches above the hearth decreased to approximately 78% below baseline.

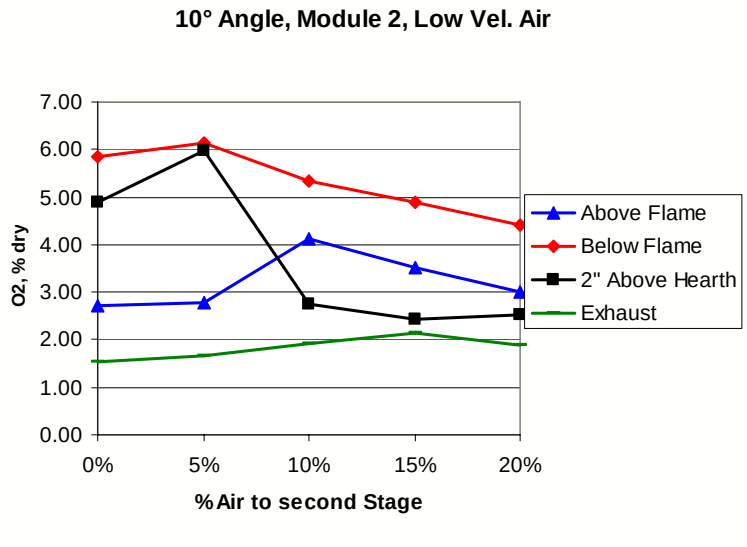


FIGURE 34 EFFECT IN MODULE 2 OF LOW-VELOCITY SECONDARY AIR INJECTION AT 10º AWAY FROM THE THERMJET BURNER

Figure 34 shows the effect in the second furnace module of introducing low-velocity secondary air above the flame at 10°. While the oxygen concentration at the exhaust remained approximately the same with increasing secondary air injection, the oxygen concentration two inches above the hearth decreased to approximately 50% below baseline.

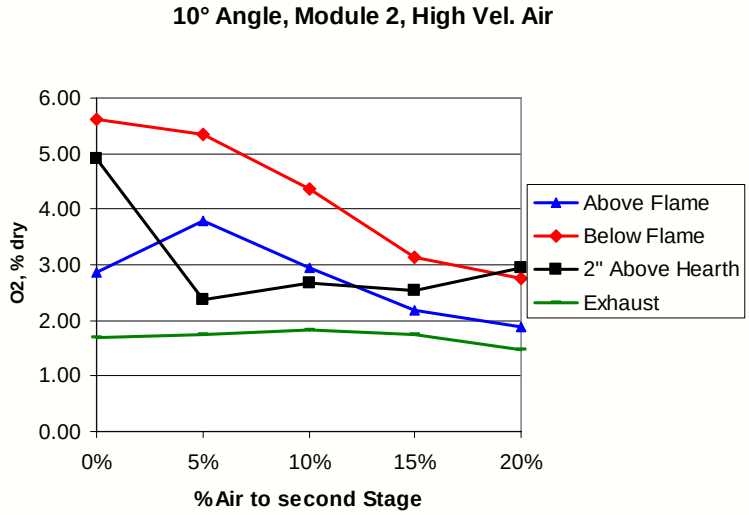


FIGURE 35 EFFECT IN MODULE 2 OF HIGH-VELOCITY SECONDARY AIR INJECTION AT 10º AWAY FROM THE THERMJET BURNER

Figure 35 shows the effect in the second furnace module of introducing high-velocity secondary air above the flame at 10°. While the oxygen concentration at the exhaust remained approximately the same with increasing secondary air injection, the oxygen concentration two inches above the hearth decreased to approximately 40% below baseline.

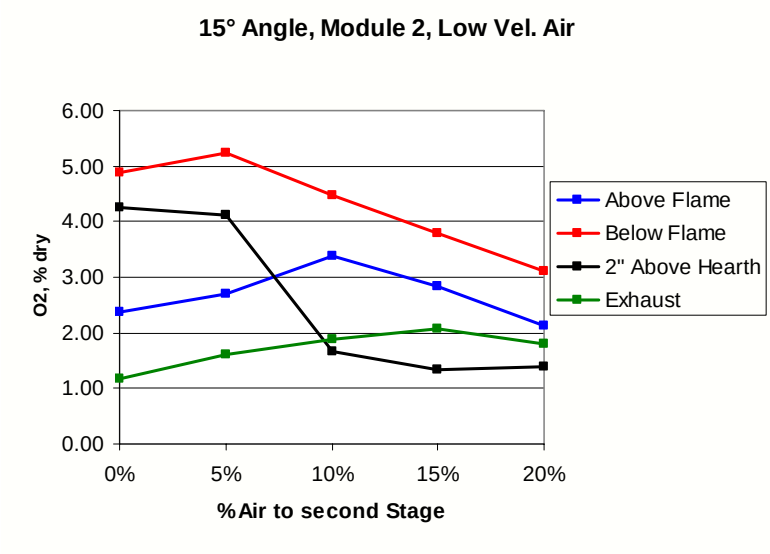


FIGURE 36 EFFECT IN MODULE 2 OF LOW-VELOCITY SECONDARY AIR INJECTION AT 15º AWAY FROM THE THERMJET BURNER

Figure 36 shows the effect in the second furnace module of introducing low-velocity secondary air above the flame at 15°. While the oxygen concentration at the exhaust remained approximately the same with increasing secondary air injection, the oxygen concentration two inches above the hearth decreased to approximately 69% below baseline.

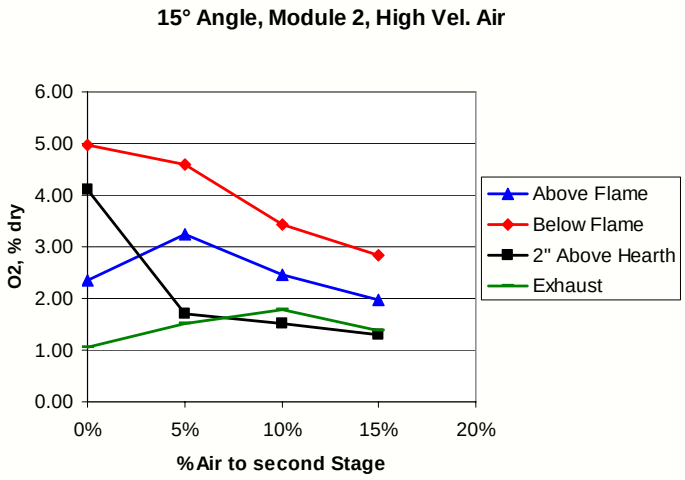


FIGURE 37 EFFECT IN MODULE 2 OF HIGH-VELOCITY SECONDARY AIR INJECTION AT 15º AWAY FROM THE THERMJET BURNER

Figure 37 shows the effect in the second furnace module of introducing high-velocity secondary air above the flame at 15°. While the oxygen concentration at the exhaust remained approximately the same with increasing secondary air injection, the oxygen concentration two inches above the hearth decreased to approximately 68% below baseline.

**$NO_x$ Emissions Reduction from Secondary Air Injection**

Figure 38shows the effect of introducing low-velocity secondary air above the flame on $NO_x$ concentrations in the furnace exhaust. The greatest $NO_x$ decrease was observed at 20% secondary air and at the 5° injection angle. The average $NO_x$ decrease for all angles at 20% secondary air was approximately 23%.

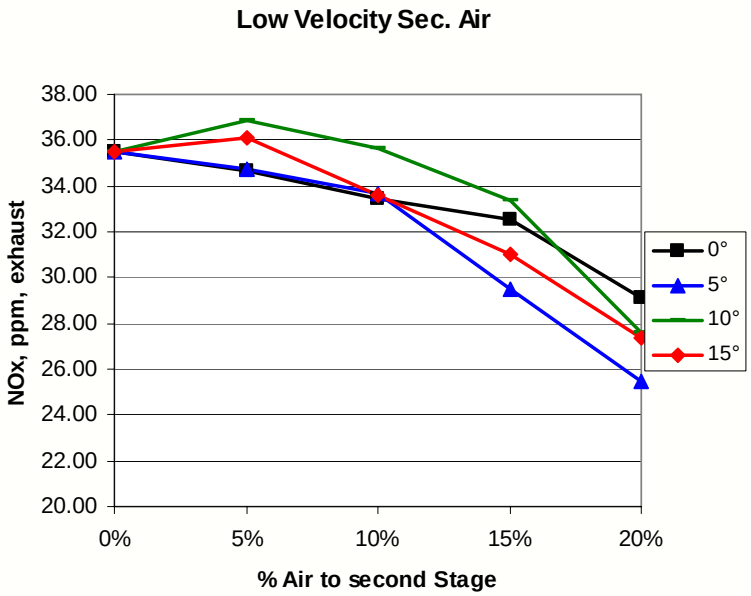


FIGURE 38 EFFECT OF LOW-VELOCITY SECONDARY AIR INJECTION ON $NO_X$ EMISSIONS FROM THE THERMJET BURNER

Figure 39 shows the effect of introducing high-velocity secondary air at all angles above the flame on $NO_x$ concentrations in the furnace exhaust. The greatest $NO_x$ decrease, averaging 23%, was observed at 20% secondary air.

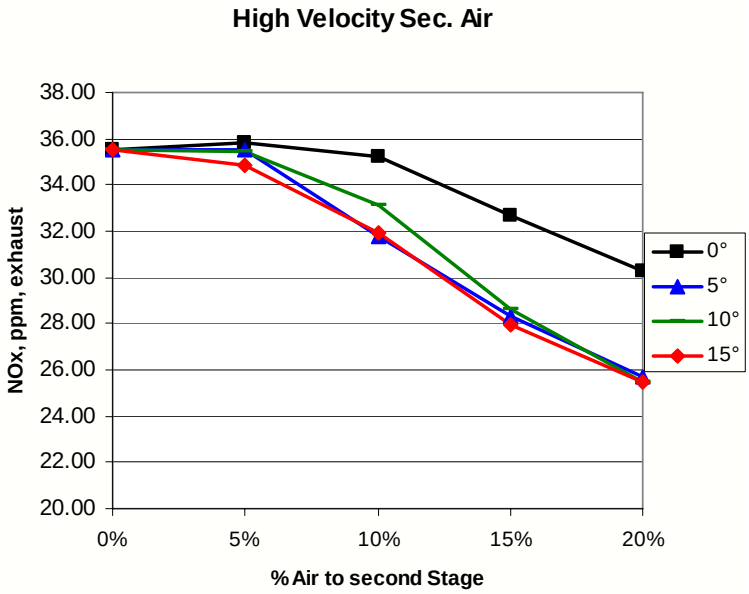


FIGURE 39 EFFECT OF HIGH-VELOCITY SECONDARY AIR INJECTION ON $NO_X$ EMISSIONS FROM THE THERMJET BURNER

**CO Emissions Reduction from Secondary Air Injection**

Figure 40 shows the effect of introducing low-velocity secondary air at all angles above the flame on CO concentration in the furnace exhaust. For angles 5, 10, and 15° there was an increase in the formation of CO due to inadequate mixing of the secondary air stream with the main flame. At 0°, CO concentrations did not change significantly.

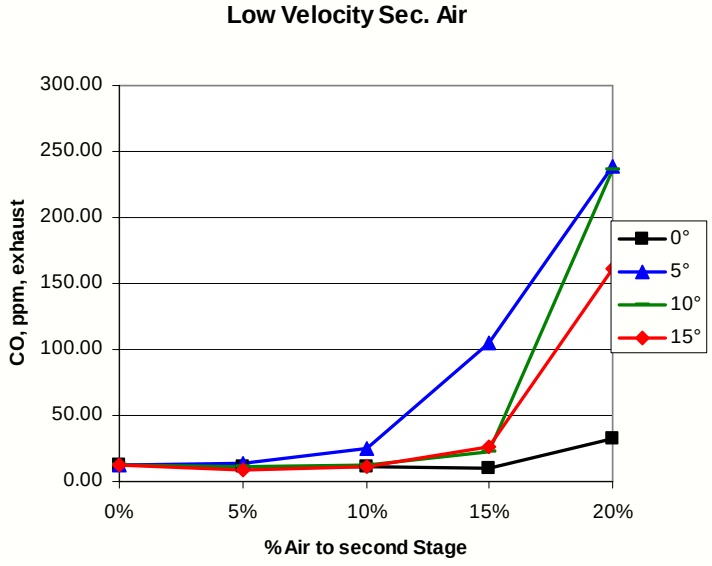


FIGURE 40 EFFECT OF LOW-VELOCITY SECONDARY AIR INJECTION ON CO EMISSIONS FROM THE THERMJET BURNER

Figure 41 shows the effect of introducing high-velocity secondary air at all angles above the flame on CO concentration in the furnace exhaust. For angles of 5º, 10º, and 15° there was an increase in the formation of CO due to inadequate mixing of the secondary air stream with the main flame. At 0°, CO concentrations did not change significantly.

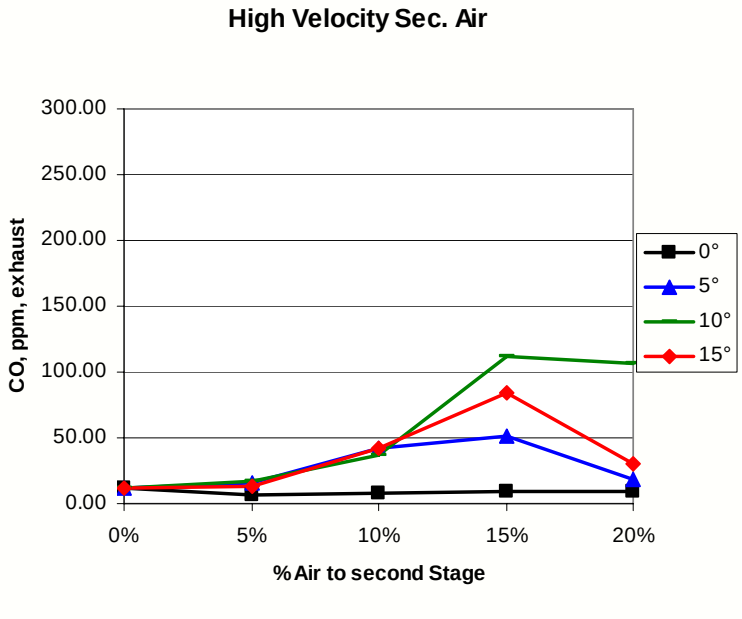


FIGURE 41 EFFECT OF HIGH-VELOCITY SECONDARY AIR INJECTION ON CO EMISSIONS FROM THE THERMJET BURNER

**Analysis of ThermJet Burner Test Results**

Introducing secondary air above the ThermJet burner reduced the concentration of oxygen near the furnace hearth by 20% to 80% for the range of conditions tested. The concentration of $NO_x$ in the exhaust was reduced by up to 25%. This was a direct effect of staging the combustion. The CO increased for secondary air injected at larger angles, which indicates that, at the larger angles, the secondary air was not mixed properly in the main combustion zone.

**Conclusions**

As shown in Table 2, the modified ThermJet burner provided promising levels of control of the oxygen concentrations near the furnace hearth. The largest amount of secondary air injected provided the greatest reduction in oxygen concentration near the furnace hearth. The data in Table 1 show that high injection angles and high air velocities also provided the largest reductions in oxygen concentration. These observations provide a direction for further development of low-dross burners.

**Table 2 Reduction of Hearth-Level Oxygen Concentration by 20% Secondary Air Injection (Percent Reduction from a Baseline of No Secondary Air Injection)**

| | Injection Angle | | | |
|---|---|---|---|---|
| **Configuration** | **0º** | **5º** | **10º** | **15º** |
| Low-velocity injection, oxygen measured in furnace module 1 | 20 | 78 | 58 | 79 |
| High-velocity injection, oxygen measured in furnace module 1 | 35 | 55 | 65 | 82 |
| Low-velocity injection, oxygen measured in furnace module 2 | 30 | 56 | 50 | 69 |
| High-velocity injection, oxygen measured in furnace module 2 | 55 | 78 | 40 | 68 |

The use of 20% secondary air injection with the ThermJet burner reduced $NO_x$ emissions from the furnace by an average (over all injection angles) of 23%. Emissions of carbon monoxide were not reduced, but neither were they significantly increased at high air flow rates

**Optical Flame Sensor Results on Modified ThermJet Burner**

The Eclipse ThermJet Burner (150 kBtu/hr max) was used for testing the filter wheel-CCD imaging system. Figure 42 shows a photograph of the burner being tested with the retrofitted quartz nozzle.

FIGURE 42: PHOTOGRAPH OF THERMJET BURNER FLAME WITH RETROFITTED QUARTZ NOZZLE

Experiments were performed by varying the percent excess air from very rich (-20%EA) to very lean (40%EA) while acquiring data from the flames using the filter wheel-CCD system. The test matrix for the burner parameters is shown in Table 3, with the corresponding flow rates.

**Table 3: ThermJet Burner Test Matrix for the Filter Wheel-CCD Imaging Sensor Testing**

| %EA | Air (l/m) | Fuel (l/m) |
|---|---|---|
| 40 | 387 | 29 |
| 30 | 359 | 29 |
| 20 | 332 | 29 |
| 10 | 304 | 29 |
| 0 | 276 | 29 |
| -10 | 249 | 29 |
| -20 | 221 | 29 |

For each flame type, two sets of filtered images were collected. The flames did not exhibit significant background radiation (no soot, and, therefore, the data was reduced using only the primary OH* and CH* transmittance filters (310 and 430 nm, respectively). This method allowed the elimination of errors due to inaccuracies that may have been introduced by the background subtraction algorithm in the developed software. The data analysis software was used to reduce the acquired data into a quantifiable form. This tool allows the user to select the range of data to analyze, using a percentage of the filtered data. It is necessary to not use very low-intensity data because that would cause large errors when taking ratios.

Figure 43 shows two sample images acquired from the ThermJet burner with the quartz nozzle. The structure of the combustion processes can be viewed within the nozzle as well as above the exit nozzle. The data presented here only represents data acquired above the exit nozzle.

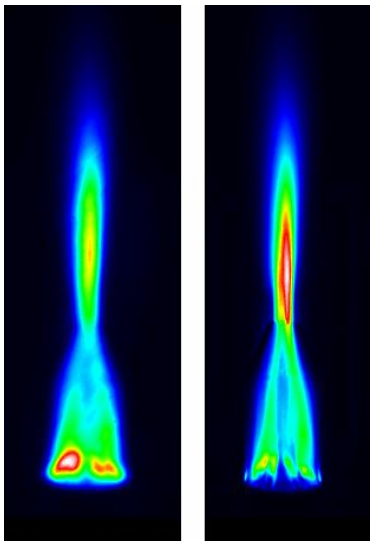

(a) (b)

FIGURE 43: OH* (A) AND CH* (B) IMAGES ACQUIRED FROM THE THERMJET BURNER

Figure 44 shows the OH*/CH* images for 5-100% of the signal data. The most important information in this image series is the relative change in color (intensity) with changing excess air.

Visually, there are no large variations between the OH*/CH* ratios images. Each image portrays data from the low to high end of the range displayed, however, the most significant difference between the images is the quantity of low and high OH*/CH* pixels. The higher %EA conditions yielded more low OH*/CH* data on the images than those with higher %EA, and vice versa.

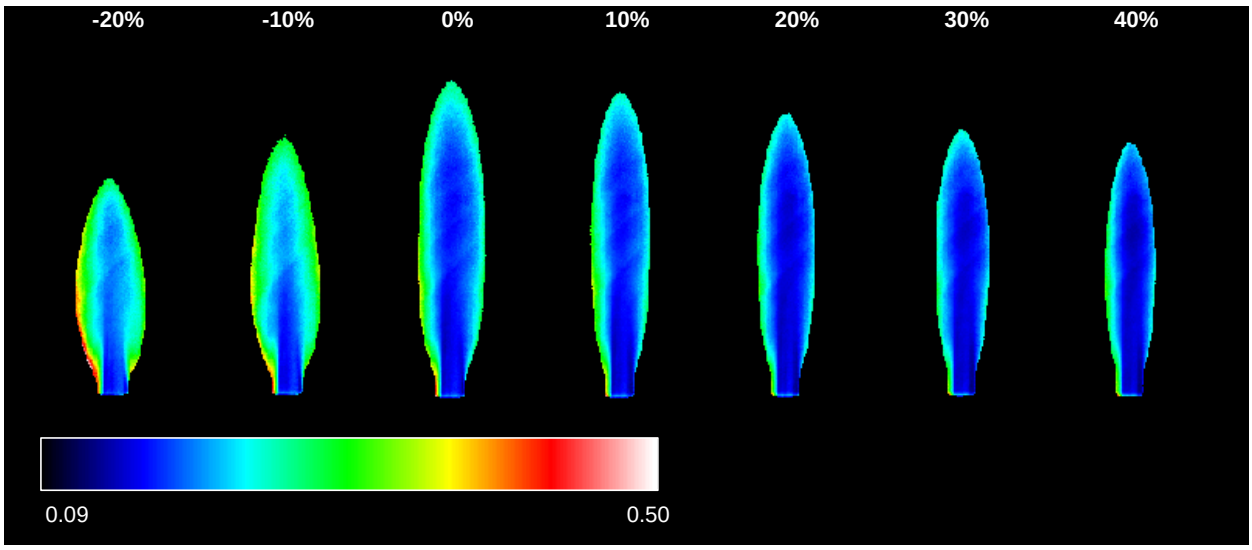


FIGURE 44: OH*/CH* RATIO IMAGES FROM THERMJET BURNER FLAMES WITH NOTED %EA; 5-100% MAXIMUM INTENSITY

The data from the image series above were averaged, and this quantified data is shown in Figure 45. The figure shows the largest changes in the OH*/CH* ratio between flames conditions of -10%EA and 20%EA. The trend of the data is somewhat opposite that found from the flat-flame experiments. Flat-flame experiments showed an increase in OH*/CH* ratio with %EA, whereas, here, the exact opposite was found. This observation emphasizes the lack of similarity between premix and nozzle-mix flame when analyzing their flame light.

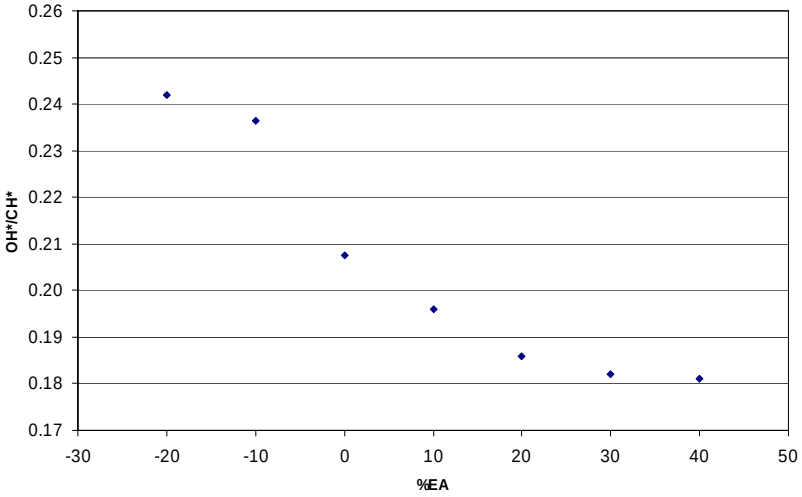


FIGURE 45: AVERAGED OH*/CH* DATA FROM THE THERMJET BURNER

Secondary air tests were also performed. Here, asymmetric fuel-rich and a fuel-lean flame sides were generated by using a secondary air nozzle on the left side of the burner. Burners with this configuration are being developed to generate asymmetric flames with a low oxygen side to help prevention oxidation of industrial furnace loads.

The test matrix is shown in Table 4. The burner excess air was held constant at 5%. The secondary air was varied between 0% and 30% secondary air (SA) to enhance the visible effect on the flame.

**Table 4: Test Matrix for Testing Secondary Air Effects on OH*/CH* Ratio Images**

| %EA | %SA | Fuel (l/m) | Primary Air (l/m) | Secondary Air (l/m) | Total Air (l/m) |
|---|---|---|---|---|---|
| 5 | 0 | 29 | 290 | 0 | 290 |
| 5 | 10 | 29 | 261 | 29 | 290 |
| 5 | 20 | 29 | 232 | 58 | 290 |
| 5 | 30 | 29 | 203 | 87 | 290 |

The series of images in Figure 46 show the change of the OH*/CH* with secondary air variance. These images were produced from the analysis of light exceeding 5% of the maximum light intensity. The images do not exhibit an observable change in the symmetry of the OH*/CH* images. There is no noticeable asymmetry increase with increasing secondary air.

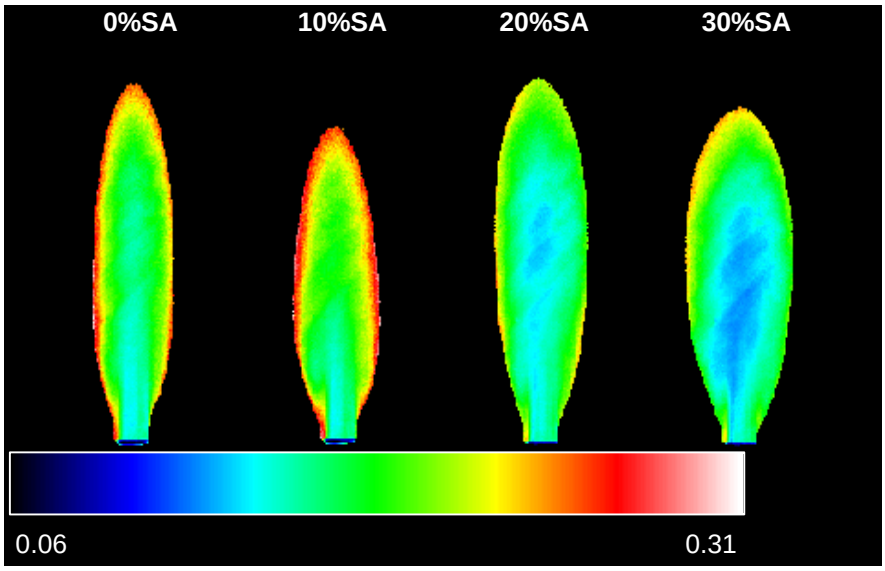


FIGURE 46: OH*/CH* RATIO IMAGES FROM THERMJET BURNER FLAMES AT VARIOUS SECONDARY AIR CONDITIONS

These images were further analyzed by averaging the left and right halves of the flame OH*/CH* data. Figure 47 shows this data. This plot does not show a trend worth noting. It appears that, rather than showing a fuel-rich and fuel-lean side of the flame, it shows a flame that is increasingly rich. This could be due to delayed mixing of the secondary air into the flame, perhaps further above the luminous section of the flame. In a furnace, the mixing properties of the gases are different, and it is possible that a correlation would be evident in that setting.

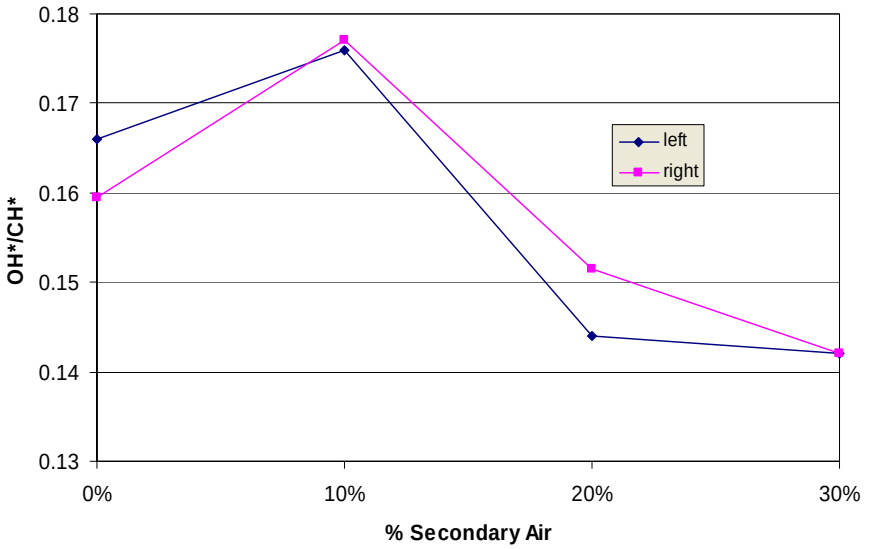


FIGURE 47: AVERAGED LEFT AND RIGHT SIDE OH*/CH* RATIO DATA AT VARIOUS SECONDARY AIR CONDITIONS

**Conclusions on Optical Flame Sensor**

The use of flame light as means to extract otherwise unattainable information shows promise for future industrial sensors. The work performed here showed that premixed flames can accurately be observed and their light correlated to the fuel/air ratio of the flame. Both spectrometer and filter-wheel systems were capable of determining the correct equivalence ratio of flat flames after a correlation was developed. In addition, premixed flames proved to be effective examples for correlating OH* spectrum light to flame temperatures for low-velocity flames. A spectrometer-CCD system provided preliminary insight into nozzle-mix burner light emissions and their relationship to fuel/air ratios. Asymmetric flames were observed spectrally, showing that flame light emission reacts to flame shape changes. Investigations using the spectrometer-CCD system with a pilot-scale nozzle mix burner within a furnace yielded results that showed a linear increase in the OH*/CH* ratio with increasing secondary air between 0 and 15% excess air. This relationship was the opposite of what was found to occur with premixed flames. Since data was only obtained from one location in the flame's reaction zone, data further upstream of the flame might yield different results. The use of the filter wheel-CCD system with an industrial high-momentum burner proved the sensor's effectiveness to observe distinct locations of flame zones. In addition, the use of a quartz nozzle with the burner yielded insight to the flame dynamics occurring within the burner. The OH*/CH* images acquired from the flames showed distinct regions of higher and lower values, proving the sensor's effectiveness in qualitatively observing differences between differing flame types. Quantified image data from testing this burner yielded a well-defined trend of decreasing OH*/CH* ratio with increasing excess air when the excess air was varied from -30% to +40%. The most distinct correlation was found for the leaner flames with excess air less than 20%.

**Laboratory Tests of Modified (5 MMBtu/hr) ThermJet Burner**

**Arrangements for Modified 5 MMBtu/hr ThermJet Burner**

The 5 MMBtu/hr flex-flame burner system was tested in the Eclipse Combustion laboratory. The burner was installed on a test furnace (see Figure 48). Four water-cooled probes were utilized to sample combustion gases in the combustion chamber and flue chamber. Two of the probes sampled 3 inches above the furnace hearth (one third and two thirds along the furnace length), one probe sampled along the flame centerline (halfway along the furnace length), and the last probe sampled in the exhaust stack. These probes were water-cooled to assure continuous operation during the test. The furnace was equipped with two type R thermocouples, the first measuring furnace refractory temperature and the second located in the bottom left sample probe location to measure furnace interior temperature.

A portable HORIBA gas analyzer (model PG-250A) was used to monitor oxygen, carbon monoxide, nitrous oxide/dioxide, and carbon dioxide concentrations at each probe location.

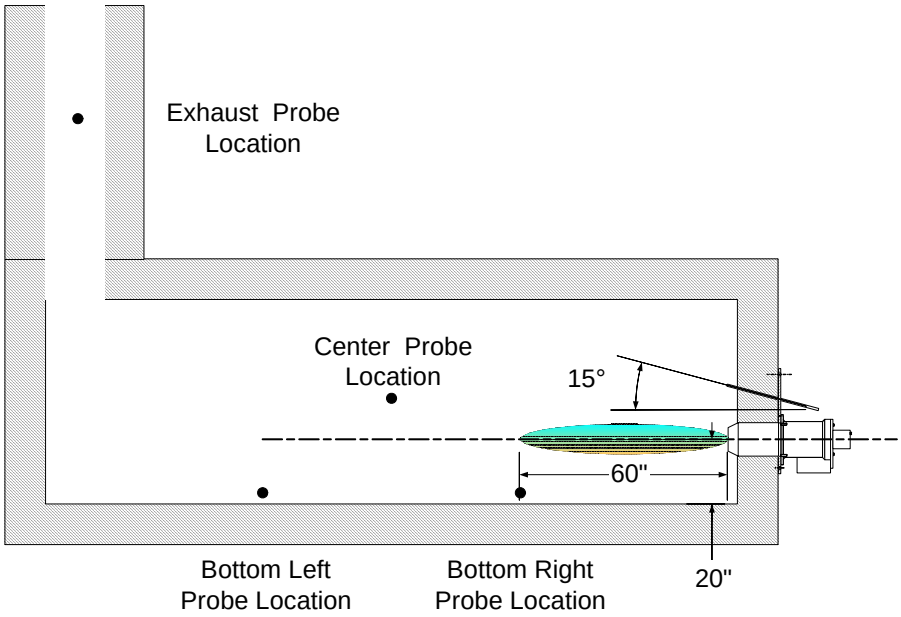


FIGURE 48 EXPERIMENTAL SETUP, THERMJET BURNER FIRING STRAIGHT INTO THE FURNACE CHAMBER, WITH SECONDARY AIR TUBE DIRECTED 15° ABOVE THE CENTERLINE

The test matrix was designed to examine the effects of secondary air introduction above the flame at 15° away from the flame and to compare the performance relative to baseline operation, where no secondary air was used. The performance was mainly determined by noting changes in the concentrations of oxygen throughout the furnace as well as $NO/NO_2$ levels in the exhaust stack. The burner was maintained at approximately 3.5 MMBtu/hr and 3-4% excess air. To avoid overheating the furnace chamber, firing was maintained for about 15 minutes at a time before shutting down to cool. During this 15-minute time period, all emissions and temperatures were recorded. Three separate tests were performed:

1. 3.5 MMBtu/hr, 3-4% excess air level, 0% secondary air.

2. 3.5 MMBtu/hr, 3-4% excess air level, 20% secondary air.
3. 3.5 MMBtu/hr, 3-4% excess air level, 30% secondary air.

The results from the Eclipse experiments are given below

**$NO_x$ in the Exhaust**

Our experiments at Eclipse yielded the following results for $NO_x$ in the exhaust as a function of secondary air injection above the flame.

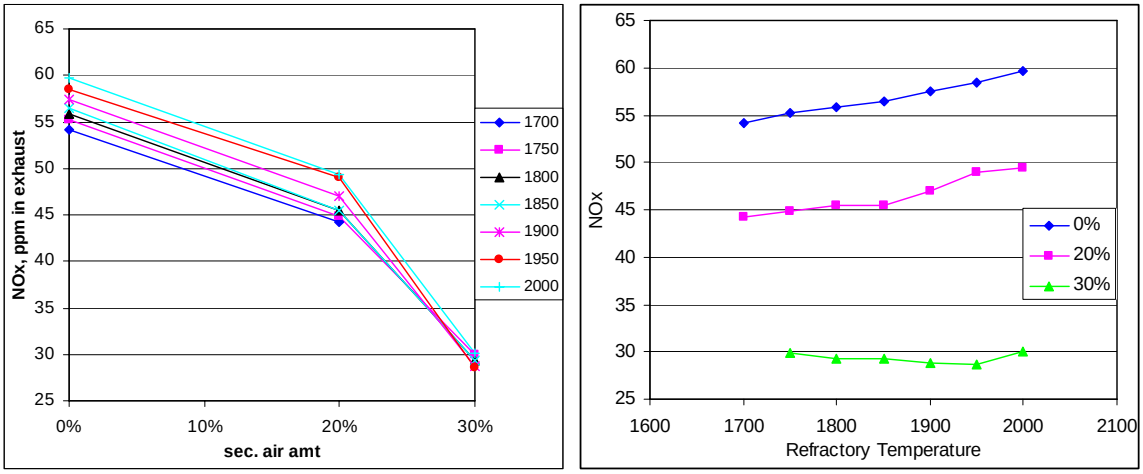


FIGURE 49 NOX LEVELS IN THE EXHAUST IN PPM FOR: (LEFT) VARIOUS FURNACE TEMPERATURES AND (RIGHT) VARIOUS SECONDARY AIR LEVELS

The left-hand chart in Figure 49 shows the reduction of $NO_x$ in the exhaust as a function of secondary air injection. The greatest reduction occurred at the highest secondary air injection (30%). Each line represents a different furnace refractory temperature, all within the range where a typical secondary aluminum reverberatory furnace operates. For all temperatures, $NO_x$ is reduced with increasing secondary air injection, while, at the mean temperature (1850°F), $NO_x$ levels were reduced by up to 48%.

The right-hand chart in Figure 49 shows the same data in a different format. For any furnace temperature, the $NO_x$ emissions in the exhaust are significantly lower for increasing secondary air injection.

**Reduction of Oxygen Near the Furnace Hearth.**

Secondary air was injected at 15° away from the flame centerline. At these conditions, the oxygen in the 3 locations varied as a function of secondary air level, as shown in Figure 50.

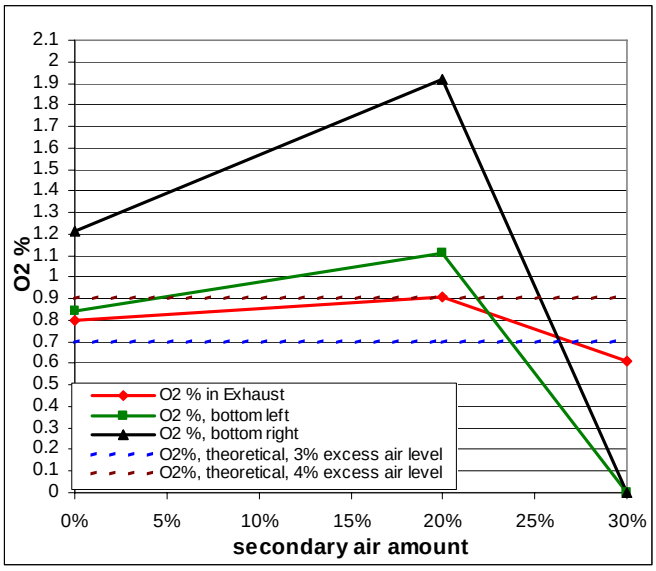


FIGURE 50 OXYGEN LEVELS (% DRY) IN ALL MEASURED LOCATIONS AS A FUNCTION OF SECONDARY AIR AT ECLIPSE'S FACILITY ON THE 5 MMBTU/HR BURNER PLATFORM

Even though the oxygen level measured at the exhaust remained approximately the same, the oxygen levels measured in the two near hearth locations exhibited an unexplained peak at 20% secondary air injection. During the 1 MMBtu/hr testing, the oxygen concentration near the hearth followed a smooth one-to-one decreasing curve (Figure 51). One explanation for this peak may be specific furnace geometry. Further discussion of possible reasons for this peak is presented in the next section. Aside from this peak, however, the overall oxygen levels near the hearth dropped to 0% when the secondary air injection was increased to 30%. At such fuel-rich conditions, it is expected that the dross formation rate will decrease.

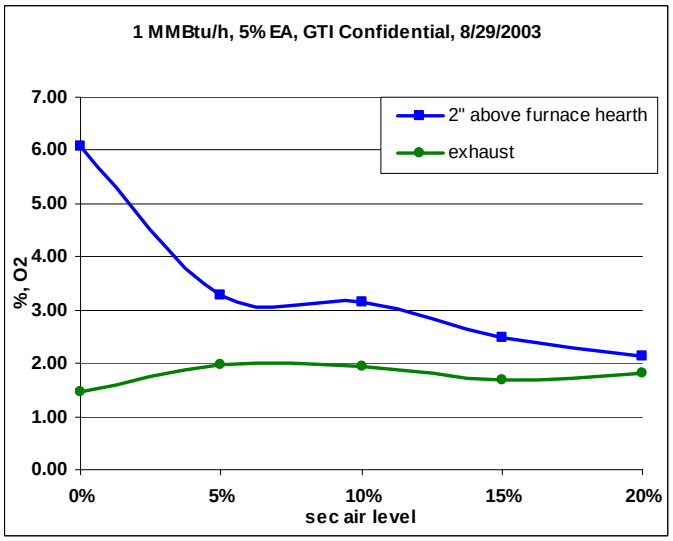


FIGURE 51 OXYGEN LEVELS (% DRY) IN ALL MEASURED LOCATIONS AS A FUNCTION OF SECONDARY AIR OBTAINED AT GTI'S FACILITY ON THE 1 MMBTU/HR BURNER PLATFORM

**CO Levels in Each Probe**

Figure 52 shows that the CO level in the exhaust does not change with increasing secondary air. As expected from the oxygen distribution profile, the CO increased beyond the measurable range in the furnace interior as the oxygen level near the hearth was driven to zero. CO levels in the exhaust remained unchanged.

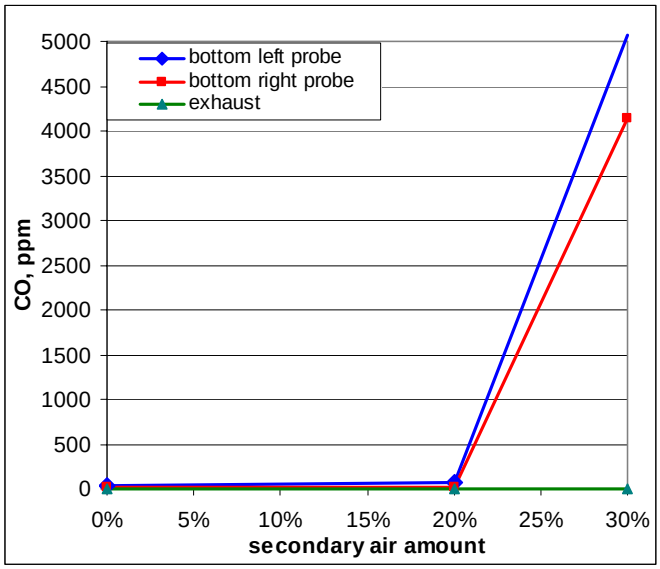


FIGURE 52 CO LEVELS (PPM DRY) AS A FUNCTION OF SECONDARY AIR FROM THE 5 MMBTU/HR BURNER PLATFORM AT ECLIPSE'S FACILITY

**Conclusions**

The 5 MMBtu/hr testing demonstrated that a significant reduction in $NO_x$ is possible by injecting secondary air near to, and above the flame. This injection of air introduces an additional stage to the combustion of the fuel gas. By subtracting main combustion air and adding it above the flame, the flame becomes more fuel rich (Figure 54), thus lowering the flame temperature, as shown in Figure 53.

NOx formation depends heavily on flame temperature. Decreasing the local excess air level decreases flame temperature and $NO_x$ formation.

The second criterion for judging the performance of the low-dross combustion system is the lowering of oxygen levels in the vicinity of the furnace hearth. The testing at Eclipse produced an undesired peak of oxygen near the hearth at 20% secondary air injection. One explanation for this peak may be found when the velocity of the secondary air stream relative to flame velocity is considered. Since the ThermJet is a high-momentum burner, the flame exit velocity is considerable, on the order of 500 ft/sec. During the 1 MMBtu/hr testing at GTI, the secondary air source was a high-pressure air compressor. The secondary air nozzle size was designed to provide an air stream comparable in velocity to the flame exit stream. Using an air compressor, however, is considered unrealistic for an industrial setting. Therefore, it was decided that, for the 5 MMBtu/hr burner platform, the air supply for the secondary air stream would have to be from the same blower used for the main burner combustion air. By using a blower for the secondary air stream, the exit velocity of this stream is less than the flame exit velocity. Figure 44 and Figure 45 show the relative difference between the secondary air stream and the flame exit velocity for the 1 MMBtu/hr and 5 MMBtu/hr burner systems, respectively.

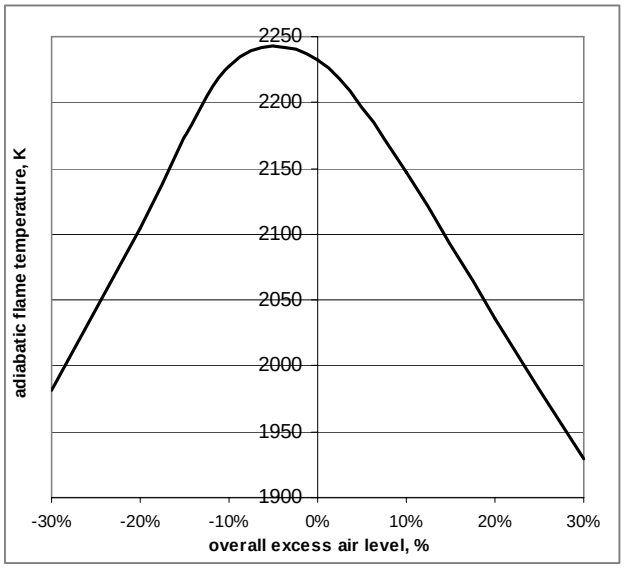


FIGURE 53 ADIABATIC FLAME TEMPERATURE AS A FUNCTION OF OVERALL EXCESS AIR LEVEL

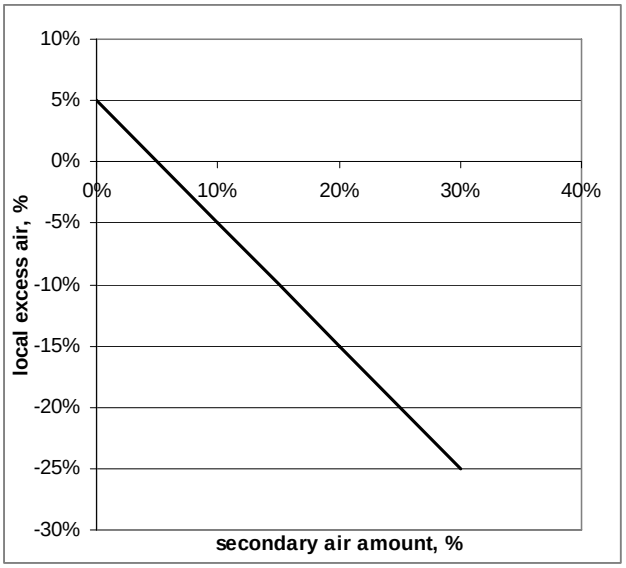


FIGURE 54 LOCAL EXCESS AIR LEVEL AS A FUNCTION OF SECONDARY AIR, 5% OVERALL EXCESS AIR

In Figure 55, the black line represents the flame exit velocity as a function of increasing secondary air level. As more secondary air is subtracted from the main combustion air and introduced as secondary air, the exit velocity of the flame decreases. The red line represents the secondary air velocity injected over the flame as a function of secondary air level (%). In Figure 56, the black line represents the flame exit velocity as a function of increasing secondary air level. As more secondary air is subtracted from the main combustion air and introduced as secondary air, the exit velocity of the flame decreases. The red line represents the secondary air velocity injected over the flame as a function of secondary air level (%).

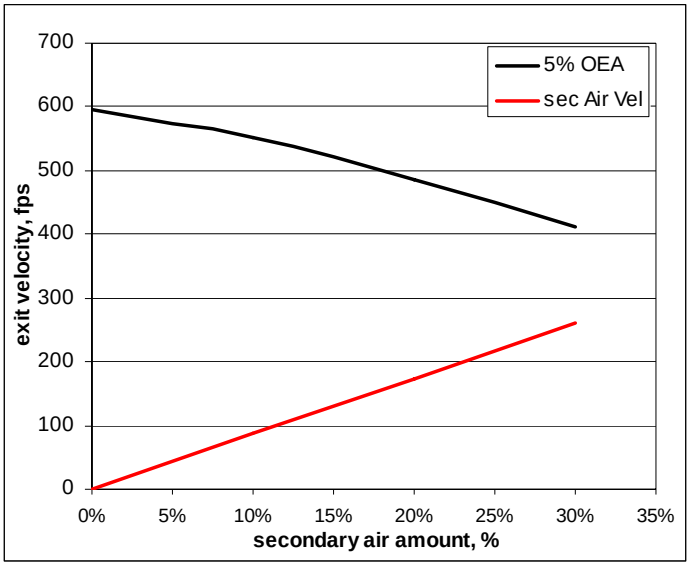


FIGURE 55 3.5 MMBTU/HR (5 MMBTU/HR BURNER PLATFORM)

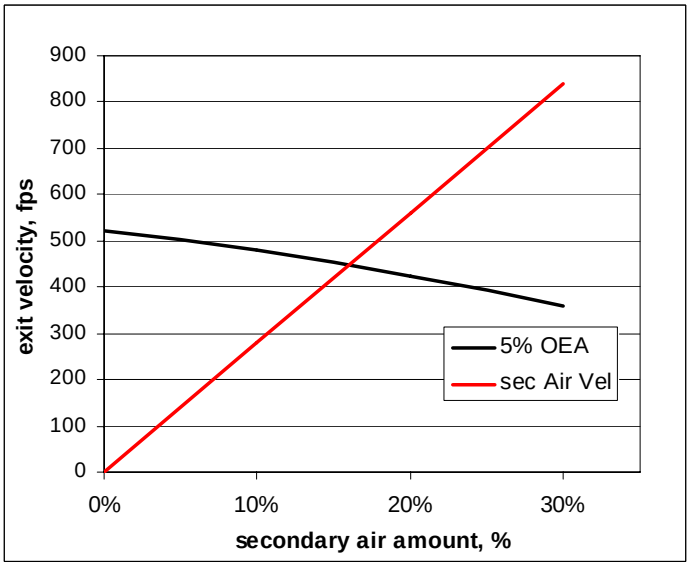


FIGURE 56 0.8 MMBTU/HR (1 MMBTU/HR BURNER PLATFORM)

As Figure 55 and Figure 56 show, the ratio of secondary air velocity to flame exit velocity for all secondary air levels was considerably higher for the 1 MMBtu/hr platform than it was for the 5 MMBtu/hr platform.

This difference in ratios may explain the peak of oxygen level near the furnace hearth at 20% secondary air injection for the 5 MMBtu/hr testing. If the secondary air velocity becomes too low with respect to the flame exit speed, the secondary air stream can become entrained in the flame sooner, compared to a secondary air stream that has comparable velocity to the flame exit speed. This early entrainment can lead to premature mixing of the two streams. If the two streams mix prematurely and completely, then the staging of the flame fails and the oxygen decrease near the furnace hearth is not achieved. The local stoichiometry of the flame becomes equal to the overall stoichiometry. A simple schematic of the possible reason is shown below in Figure 57 and Figure 58:

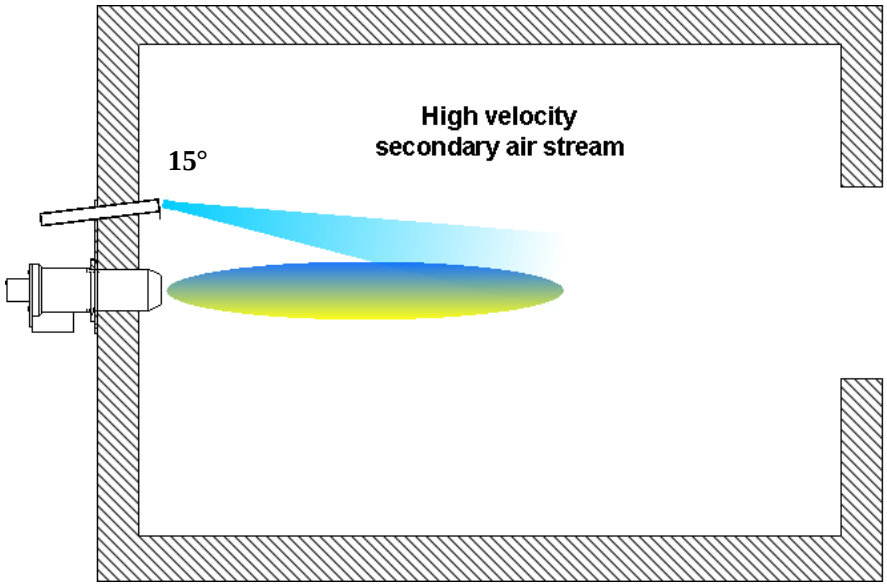


FIGURE 57 SECONDARY AIR STREAM VELOCITY HIGH ENOUGH TO AVOID RAPID MIXING

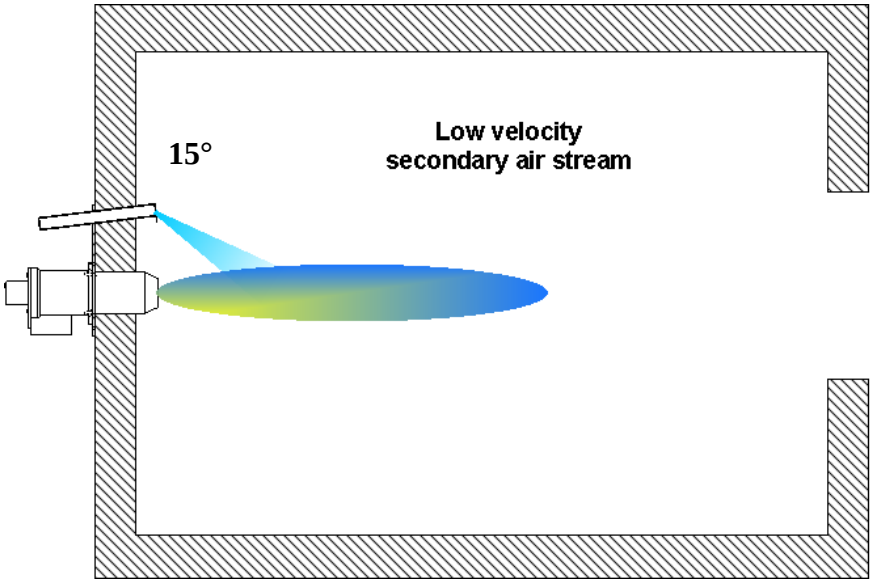


FIGURE 58 SECONDARY AIR STREAM VELOCITY TOO LOW TO PREVENT RAPID MIXING
FIELD TEST OF MODIFIED (5 MMBTU/HR) THERMJET BURNER

**WORK COMPLETED IN PHASE II, TASKS 10-15**

**Arrangements for Field Testing of Modified 5 MMBtu/hr ThermJet Burners**

**Experimental Arrangement**

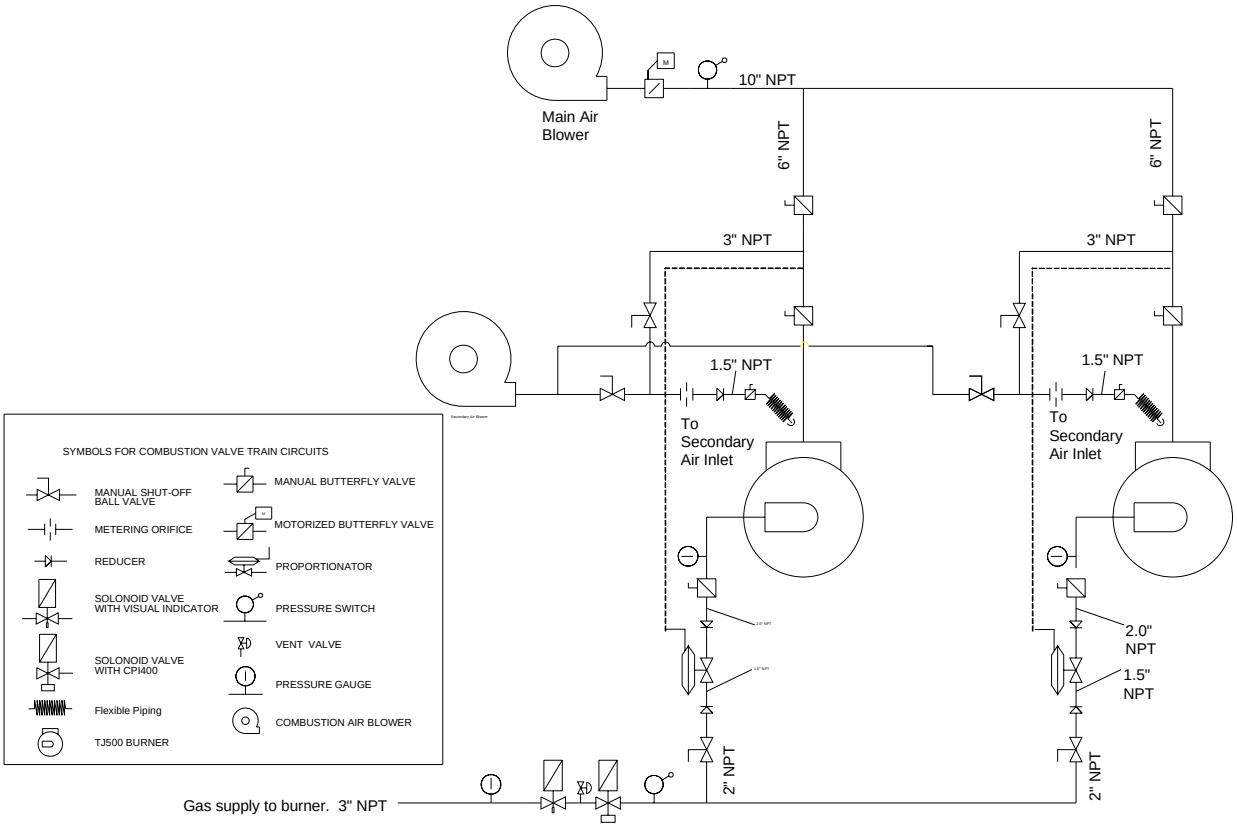


FIGURE 59 EXPERIMENTAL ARRANGEMENT AT THOROCK METALS

The reverberatory furnace at Thorock Metals is equipped with two high-momentum Eclipse Combustion TJ-500 burners capable of 10 MMBtu/hr total combined firing rate. Main combustion air is distributed evenly and is provided by a 15-hp NYB combustion blower. The secondary air stream is supplied to both burners by an additional blower. As the main combustion air is decreased, the secondary air stream is increased to maintain the same overall air/fuel ratio. Figure 59 is a schematic of the process.

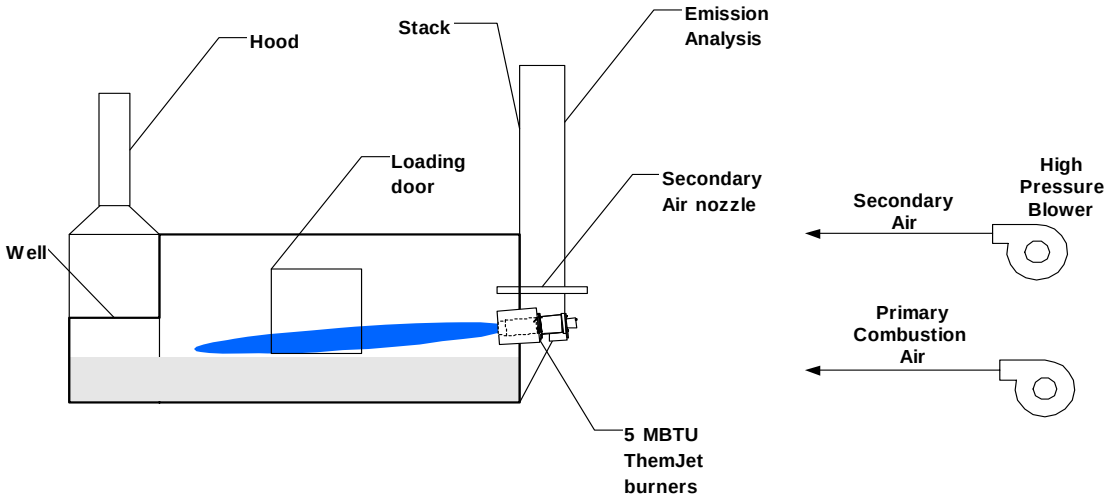


FIGURE 60 FURNACE LAYOUT

**Description of Equipment**

4. Two TJ-500 burners (5 MMBtu/hr each)
5. NYB combustion blower to be used as primary combustion air supply. Complete with a 15 hp, 220/440 volts, 3 ph, 60 Hz. 3450 rpm open drip-proof motor and filter box. Capacity 2200 cfm @ 30 inches w.c. pressure.
6. Control equipment: Consists of a NEMA 12 enclosure. The control panel shall interface with the existing panel that has the temperature high limit and flame safety system. A weekend controller shall be added with switches and lights.
7. Portable gas analyzer, HORIBA model PG-250, capable of detecting and measuring $O_2$, $CO_2$, $NO_x$, $SO_2$, and CO.
8. High-pressure blower to be used as secondary air supply. Lamson Model 3108 AB belt-drive air blower, with 25 HP TEFC motor.
9. Laptop computer for data acquisition.

**Furnace Operation**

The following excerpt was written by the head engineer at Thorock Metals and describes a typical work cycle:

"Starting with a furnace that has a small heel of between 1,000 to 4,000 lbs., an initial charge of 4,000 to 20,000 lbs. of clean scrap is placed into the hearth and well of the furnace. The furnace is then turned on. Every 20 to 30 minutes, a charge of 500 to 1,500 lbs. of clean scrap is put in the well. Once the bottom of the arch door submerges into the melt and seals the well from the hearth, dealer scrap and additives can be charged in, and drossing-off can occur when necessary. The first dross removal typically occurs between 9:00 to 11:00 P.M. As the level of the furnace increases, the rate of charge increases also. Every 30 to 40 minutes, the charge can be as much as 3,000 to 5,000 lbs. By 2:00 to 3:30 A.M., the furnace is nearly full (enough capacity only for alloying additives). At this point, any residual solid iron is removed from the furnace. The alloying additives are then mixed in and a sample coupon is taken for analyses. Once the melt is in spec and the temperature is at a proper pouring temperature, the furnace is tapped-out. The pour takes approximately 6.5-7 hours. During the first 4-5 hours of the pour an additional 25,000 to 35,000 lbs. of alloyed clean scrap is charged. The pour is finished by 2:30 to 5:30 P.M., leaving a heel of 0 to 4,000 pounds (The amount of residual "heel" depends on whether or not it is the end of the week and/or whether or not the furnace is transitioning to a new alloy). Again, an initial charge of 4,000 o 20,000 lbs. is put into the furnace and the production cycle repeats to the end of the week (Saturday)."

**Furnace Photographs**

FIGURE 61 SIDE VIEW OF THE FIELD EXPERIMENT FURNACE AT THOROCK METALS

FIGURE 62 PRIMARY BLOWER (LEFT) AND SECONDARY BLOWER (RIGHT) USED TO PROVIDE THE PRIMARY COMBUSTION AIR AND SECONDARY INJECTION AIR TO THE BURNERS

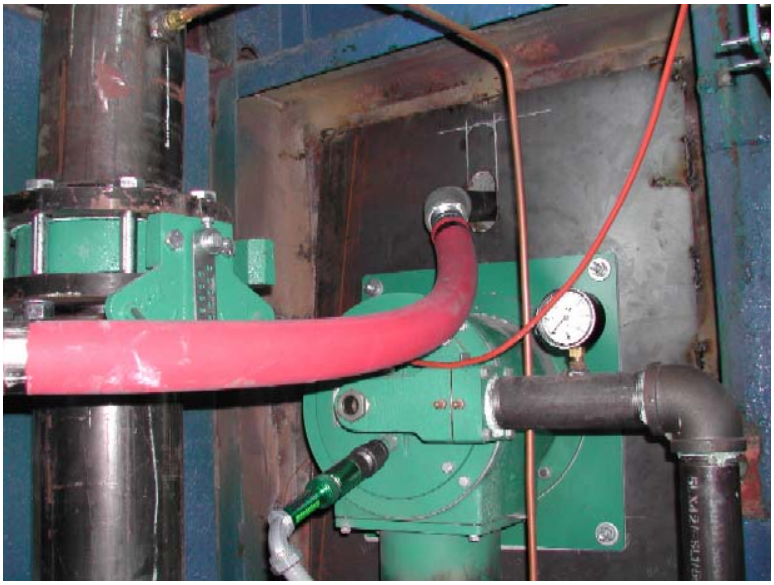

FIGURE 63 SECONDARY AIR INJECTION PORT (ABOVE THE BURNER ASSEMBLY). THE INJECTION ANGLE IS VARIABLE, AND THE SECONDARY AIR NOZZLE CAN BE REPLACED TO CHANGE THE INJECTION AIR EXIT VELOCITY.

FIGURE 64 NEWLY INSTALLED HIGH-MOMENTUM THERMJET BURNERS FIRING AT 70% CAPACITY

**Results on the 5 MMBtu/hr Field Test Platform**

**$NO_x$ in the Exhaust**

Figure 65 presents results of the $NO_x$ reduction experiments conducted at Thorock Metals. Baseline $NO_x$ emissions were sampled directly from the stack approximately 6 feet up from the burner level. The baseline $NO_x$ value was calculated as an average of a three-hour continuous recording. $NO_x$ emissions were also recorded electronically for approximately 30 minutes for each secondary air case. Higher percentages of secondary air yielded lower $NO_x$, as shown in Figure 65. Higher percentages of secondary air injection resulted in stronger $NO_x$ reduction. An angle of 10 degrees was only slightly better for $NO_x$ reduction than a 15-degree angle, and both provided a reduction of roughly 30% with 20 percent of air provided by the secondary air lance.

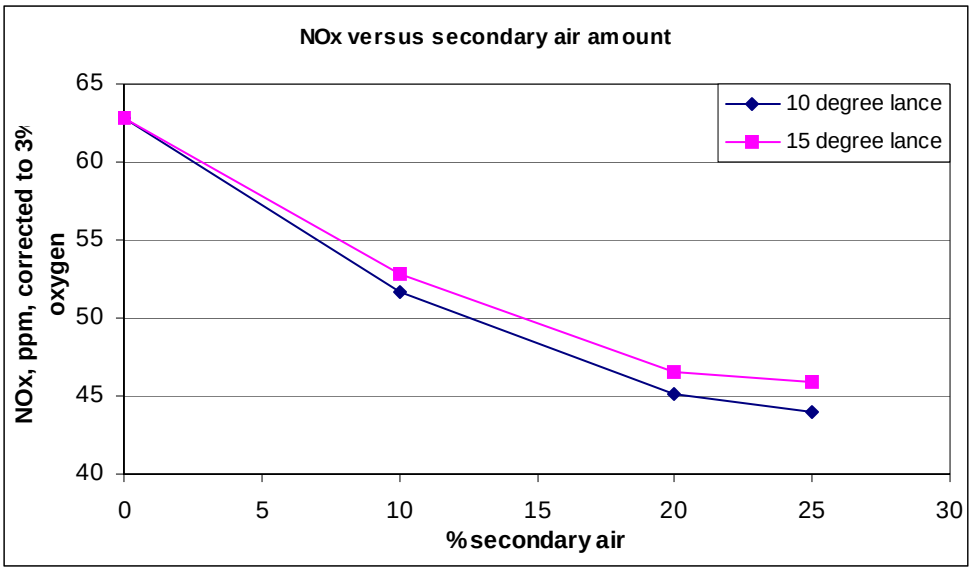


FIGURE 65 NOX IN THE FURNACE EXHAUST AT 2 INJECTION ANGLES

A comparison of CO and $O_2$ levels in the exhaust gas showed no significant variation with secondary air injection level. This confirms that combustion was complete in the furnace and there was no change in the overall air-to-fuel ratio (Figure 66). A change in air-to-fuel ratio can alter $NO_x$ production. Since this ratio was unchanged, the data clearly indicate that the decrease in $NO_x$ production was a direct result of changes in the secondary air level.

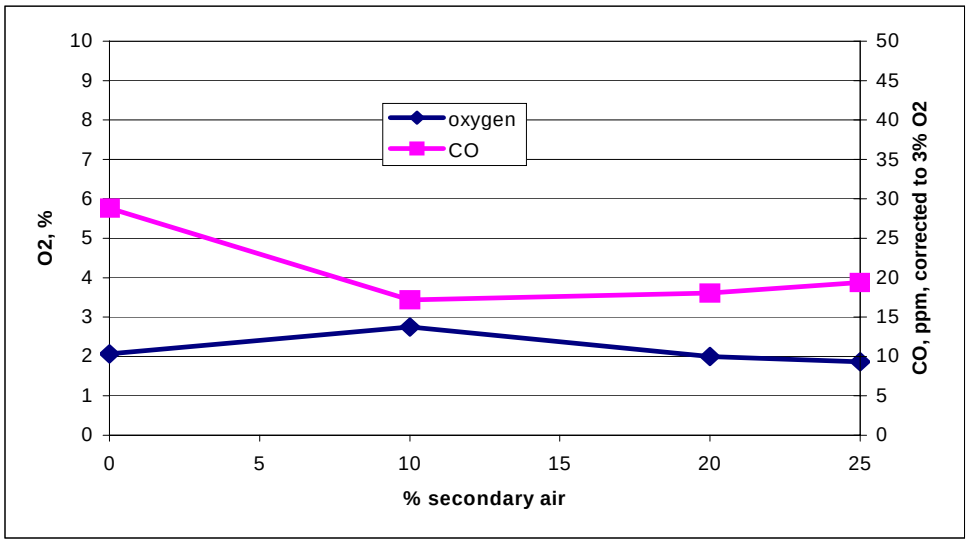


FIGURE 66 OXYGEN AND CO LEVELS IN THE EXHAUST AT A 10° INJECTION ANGLE

**Dross Formation Obtained Per Work Cycle**

Figure 67 summarizes the percent dross formation (percentage of raw material reacting to produce dross) for each work cycle.

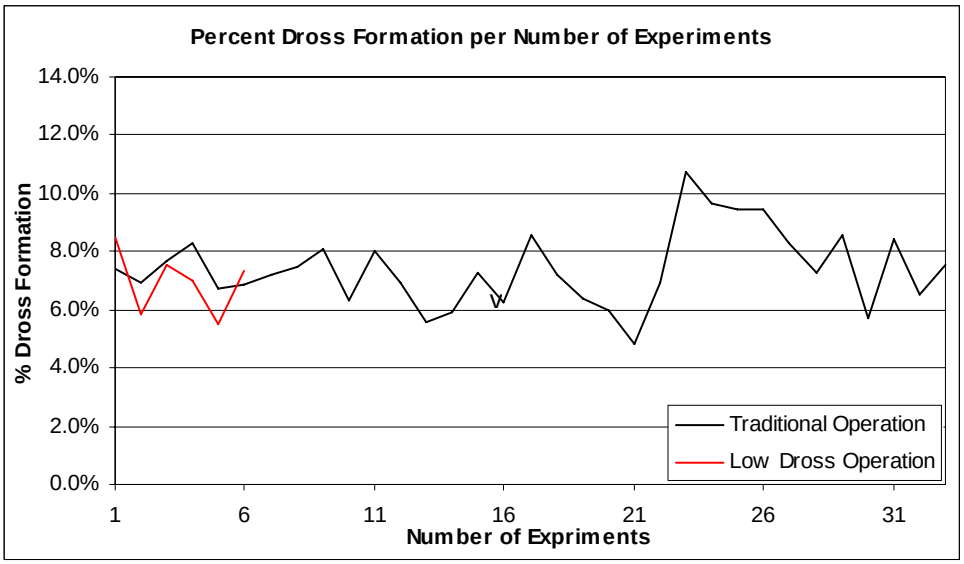


FIGURE 67 PERCENT DROSS FORMATION PER WORK CYCLE

In traditional furnace operation, dross formation was 7.4% ±0.44% (at the 95% confidence level).

In low-dross mode operation, dross formation was 6.9% ±0.89% (at the 85% confidence level).

**Fuel Consumption per Work Cycle**

Figure 68 summarizes the percent dross formation (percentage of raw material reacting to produce dross) for each work cycle.

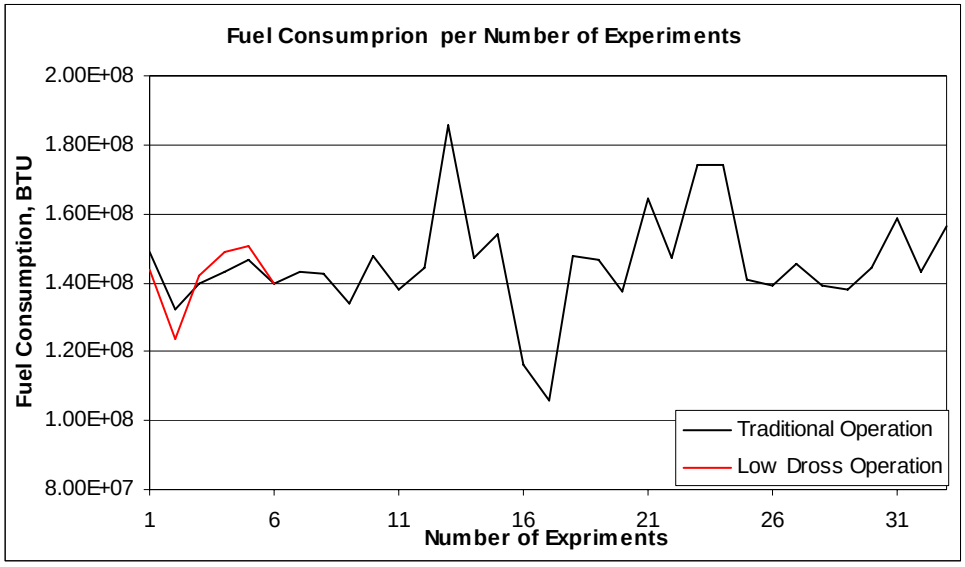


FIGURE 68 FUEL CONSUMPTION PER WORK CYCLE

In traditional furnace operation, fuel consumption was 146 ±5.1 MMBTU per test point (at the 95% confidence level)

In low-dross mode operation, fuel consumption was 141 ±7.8 MMBTU per test point (at the 95% confidence level)

**Analysis of Results**

Based on the present results, significant dross reduction was not achieved with the current configuration. Even though the average dross formation is approximately 7% lower when the low-dross mode was used, the confidence interval of this sample does not allow us to conclude that the 25% secondary air case decreases dross formation. However, the fuel consumption and production rate remained the same, and we can therefore conclude that secondary air staging can be utilized to achieve significant NOx reduction and possibly dross reduction without any loss of the furnace efficiency.

**Recommendations**

In order to complete this R&D, further testing is required on the 5 MMBtu/hr field test unit. We believe that dross reduction can be achieved by deeper staging of the flame, i.e., higher percentages of secondary air introduced above the flame. The current configuration only allows a maximum of 25% secondary air injection.